Aquarius Services Corp.
17 Pokahoe Drive
Sleepy Hollow, NY 10591
USA

Phone: +1 (914) 366-8875
Fax: +1 (914) 366-8876
e-mail: Stras69@worldnet.att.net

Advanced Nuclear Technology
Uppsala Science Park
SE-751 83, Uppsala
SWEDEN

Phone: +46-(0) 18-50 66 80
Fax: +46-(0) 18-50 66 85
e-mail: Ant@ant.se

Hydriding Mechanisms and Impact on Fuel Performance

Brian Cox and Peter Rudling

Contents

1 INTRODUCTION

2 FUNDAMENTALS OF HYDROGEN AND HYDRIDES IN ZIRCONIUM ALLOYS

3 HYDROGEN PICKUP MECHANISM

4 REDISTRIBUTION AND REORIENTATION OF HYDRIDES IN ZIRCONIUM ALLOYS

5 PARAMETERS IMPACTING BWR AND PWR HYDRIDING PICKUP BEHAVIOUR

6 INFLUENCE OF HYDRIDES ON MATERIAL PERFORMANCE

6. REFERENCES

1 INTRODUCTION

Hydrogen in zirconium alloys may influence crucial material properties such as dimensions, mechanical, corrosion and creep performance of fuel claddings, spacer and fuel channels. It has been shown in the open literature that hydrides may decrease the Zircaloy ductility and impact toughness. There have also been a number of recent investigations showing that hydrides may accelerate the uniform corrosion rate. Also, hydrogen/hydrides will in some cases influence the material creep rate. However, today there is no clear picture on whether hydrogen/hydrides increases or decreases the Zircaloy creep rate. The objective of this proposed in-depth topic is to minimise the risk of unexpected material behaviours in the future related to hydrogen pick-up and hydrogen redistribution, that could result in fuel related problems. The objective will be met by the development of a better mechanistic understanding of the steam/water Zircaloy hydriding and hydrogen redistribution processes. This understanding would facilitate the possibility to predict the in-pile hydriding tendency of the currently used commercial materials at high fluence levels.

The objective of this special topical report has been prepared within the ZIRAT-5 program is to provide members with the basic understanding of the hydrogen pickup and redistribution mechanisms involved and the impact of hydriding on fuel performance. The report covers the range from basic information to current knowledge and is written and explained in such a way that even engineers and researchers not familiar with the topic can easily follow the report, find and grasp the appropriate information. This means that the report could be used by the organisation in the training of their internal staff.

The report starts with some basic data on hydrogen and hydrides in zirconium alloys, section 2. Section 3 and 4 deals with the hydrogen pickup and redistribution mechanisms, respectively. Section 5 covers the parameters impacting the hydrogen pickup fraction while section 6 provides information on how hydrogen and hydrides in the zirconium alloy may impact fuel performance. Section 7 provides the references.

2 FUNDAMENTALS OF HYDROGEN AND HYDRIDES IN ZIRCONIUM ALLOYS

2.1 BASIC PROPERTIES

2.1.1 Solubility

Zirconium is an "exothermic occluder" of hydrogen, which means that hydrogen is more stable in solution in the α - Zr matrix than it is as hydrogen gas. The heat of solution is given by the difference between the partial molar free energy of hydrogen in the α - Zr phase ($F°_{H(\alpha)}$) and the molar free energy of hydrogen in the gas phase ($F°_{H2(g)}$). *Table 2-1* shows that this heat of solution increases as the temperature decreases *Ref. 1*. This is the factor which causes hydrogen in α - Zr to diffuse down a temperature gradient, since hydrogen is more stable in solution at the lower temperature.

Table 2-1 Heat of solution of hydrogen in α- Zr

Temp., °C	$\bar{F}°_{H(\alpha)} - \frac{1}{2}F°_{H_2(g)}$, cal/g-atom	Temp., °C	$\bar{F}°_{H(\alpha)} - \frac{1}{2}F°_{H_2(g)}$, cal/g-atom
700	+247	300	−5,540
600	−1,155	200	−7,108
500	−2,650	100	−8,692
400	−4,020	0	−10,291

The pressure of hydrogen gas which is in equilibrium with any particular mole fraction [M_H] of hydrogen in solution in α- Zr is given by:-

$$p_{H_2} = \left(\frac{M_H}{2 - M_H}\right)^2 \exp \frac{\left[\bar{F}°_{H(\alpha)} - \frac{1}{2}F°_{H_2(g)}\right]}{RT}$$

Measured isotherms for the Zr/H system are shown in Figure 2-1 from the measurements of *Hall, Martin and Rees, Ref. 2*.

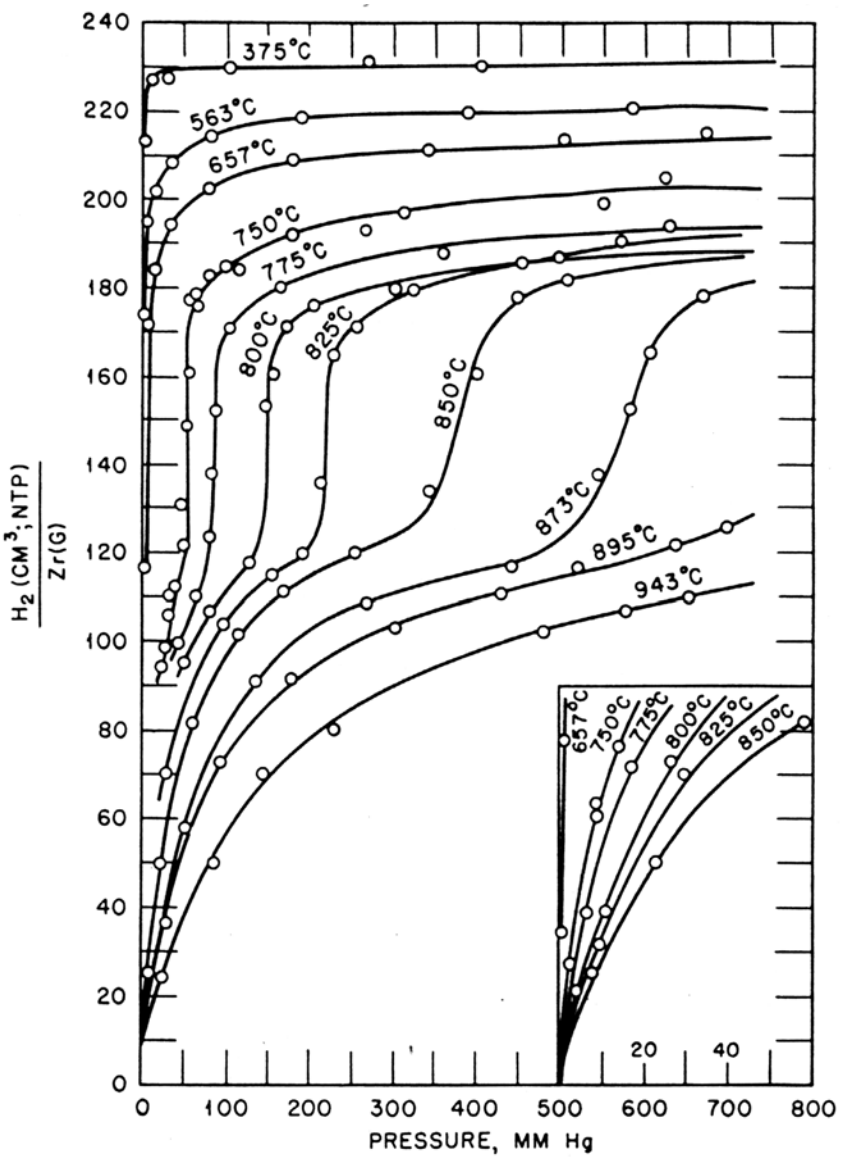

Figure 2-1: Isotherms for compact zirconium sample; 0.023 atom of oxygen per atom of zirconium. Whole series on sample of 0.04093 g with duplicate sets of points for 750°C. Inset, initial portions of isotherms on expanded pressure scale.

The inflections in these curves delimit the two-phase region where an hydride phase is precipitated in the α- Zr matrix. There are three known zirconium hydride phases (γ, δ and ε), although only the last two are typically shown in the phase diagram of the Zr/H system Figure 2-2 *Ref. 3*.

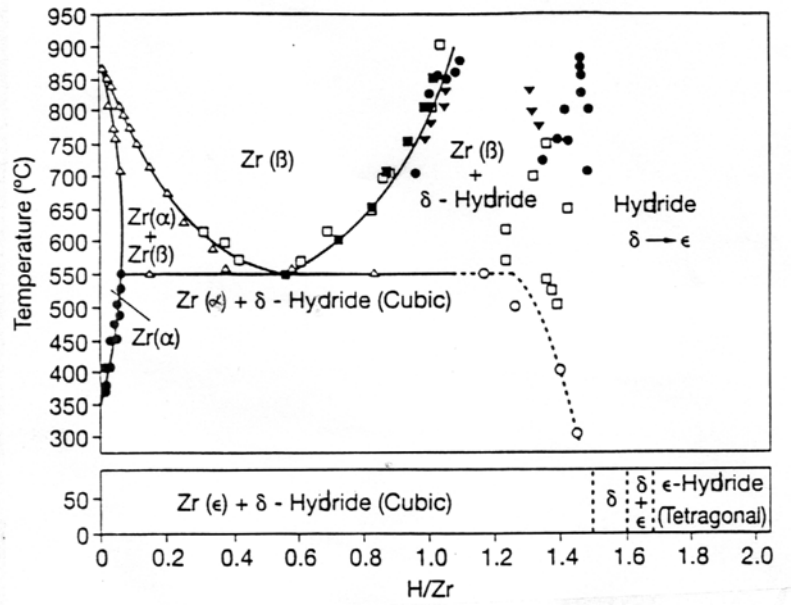

Figure 2-2: The Zirconium - hydrogen Phase Diagram

This is because the γ–ZrH phase was long regarded as being a metastable phase. It was well known, however, that the γ–ZrH and δ–$ZrH_{1.66}$ phases were often observed to co-exist in Zr alloy specimens when they were examined microscopically or by neutron diffraction. It was assumed that some impurity was perhaps stabilising the γ–ZrH phase in these circumstances. It was recently established, however, that when Zr alloy specimens were cooled the δ–$ZrH_{1.66}$ phase was the one which precipitated. However, below a temperature of 180°C this δ–phase began a slow transformation to γ–phase, Figure 2-3. Since specimens are usually studied at room temperature, and, generally, many hours after the initial cooling process, a fraction of the δ–phase would have been transformed to the γ–phase, *Ref. 4*. The various hydride phases can be distinguished from their diffraction patterns, *Table 2-2*.

(a)

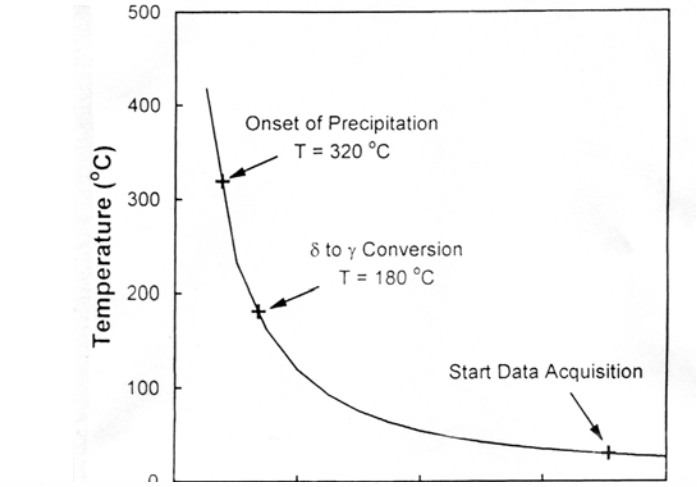

(b)

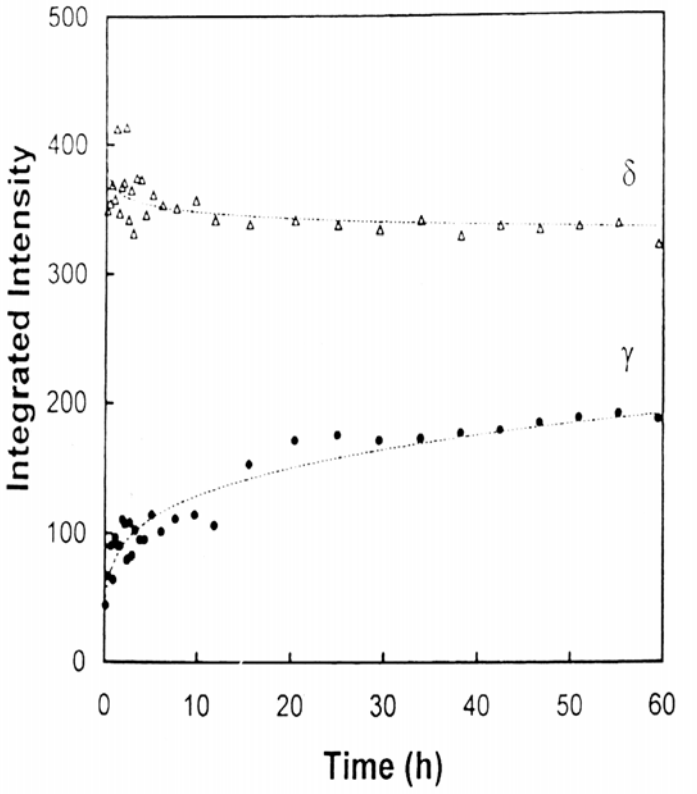

Figure 2-3: Transformation of γ–$ZrH_{1.66}$ to γ–ZrH at low temperature, (a) cooling curve for specimen in this neutron diffraction experiment, (b) kinetics of δ to γ hydide transformation in Zr-2.5Nb at 17°C after being cooled from 450°C.

Table 2-2: X-ray diffraction patterns of γ, δ and ε–Zr hydrides

COMPARISON OF X-RAY DATA

γ-ZrH			δ-ZrH$_x$			ε-ZrH$_2$		
a = 4.61 c = 4.96 c/a = 1.076			a = 4.781			a = 4.980 c = 4.450 c/a = 0.894		
Ref.: Whitwham			Ref.: Whitwham			Ref.: NBS #8944		
hkl	d	i	hkl	d	i	hkl	d	i
111	2.725	s	111	2.76	s	111	2.7608	100
002	2.480	m	200	2.39	m	200	2.4886	30
200	2.305	m	220	1.69	vs	002	2.2248	12
202	1.69	w	311	1.44	s	220	1.7599	12
220	1.63	w	222	1.38	w	202	1.6587	18
113	1.47	m	400	1.20	vw	311	1.4843	20
311	1.40	w	331	1.095	m	113	1.3804	8
222	1.36	m	420	1.07	m	222	1.3666	8
004	-	-	422	0.975	w	400	1.2443	2
400	-	-	511/333	0.92	w	331	1.1346	4
204	-	-	440	0.845	w	420	1.1128	4
331	1.06	w	531	0.81	w	313	1.0863	4
402	-	-	442	0.795	w	402	1.0797	6
420	1.03	vw				204	1.0155	2
224	-	-				422	0.9955	6
422	0.95	w				511	0.9537	4
333	0.91	vw				224	0.9403	2
511	-	-				333	0.9204	2
315	0.82	w						
424	-	-						

Two different solubilities for hydrogen in Zr are often referred to in the literature; the "maximum solubility" and the ‘terminal solid solubility’ (T.S.S.). The first is the maximum amount of hydrogen that can be absorbed under the given conditions of temperature and hydrogen pressure, and involves the conversion of the material completely to a solid Zr hydride phase (in the limit). The second solubility (T.S.S.) is the maximum amount of hydrogen that can be contained in the Zr matrix without the precipitation of a second (hydride) phase. Since the degradation of the material properties only ensues when a second-phase hydride is precipitated, it is this latter solubility which has the greatest practical importance.

Figure 2-4 shows the preferred sites for hydride precipitation. The equilibrium values of T.S.S. in pure Zircaloy from the work of *Kearns, Ref. 5* are shown in Figure 2-5.

Figure 2-4: Hydride precipitates occupying all common preferred sites in large-grained Zry-2. These sites are grain boundaries (1), twin boundaries (2), habit planes in the matrix (3), and habit planes between twins (4)

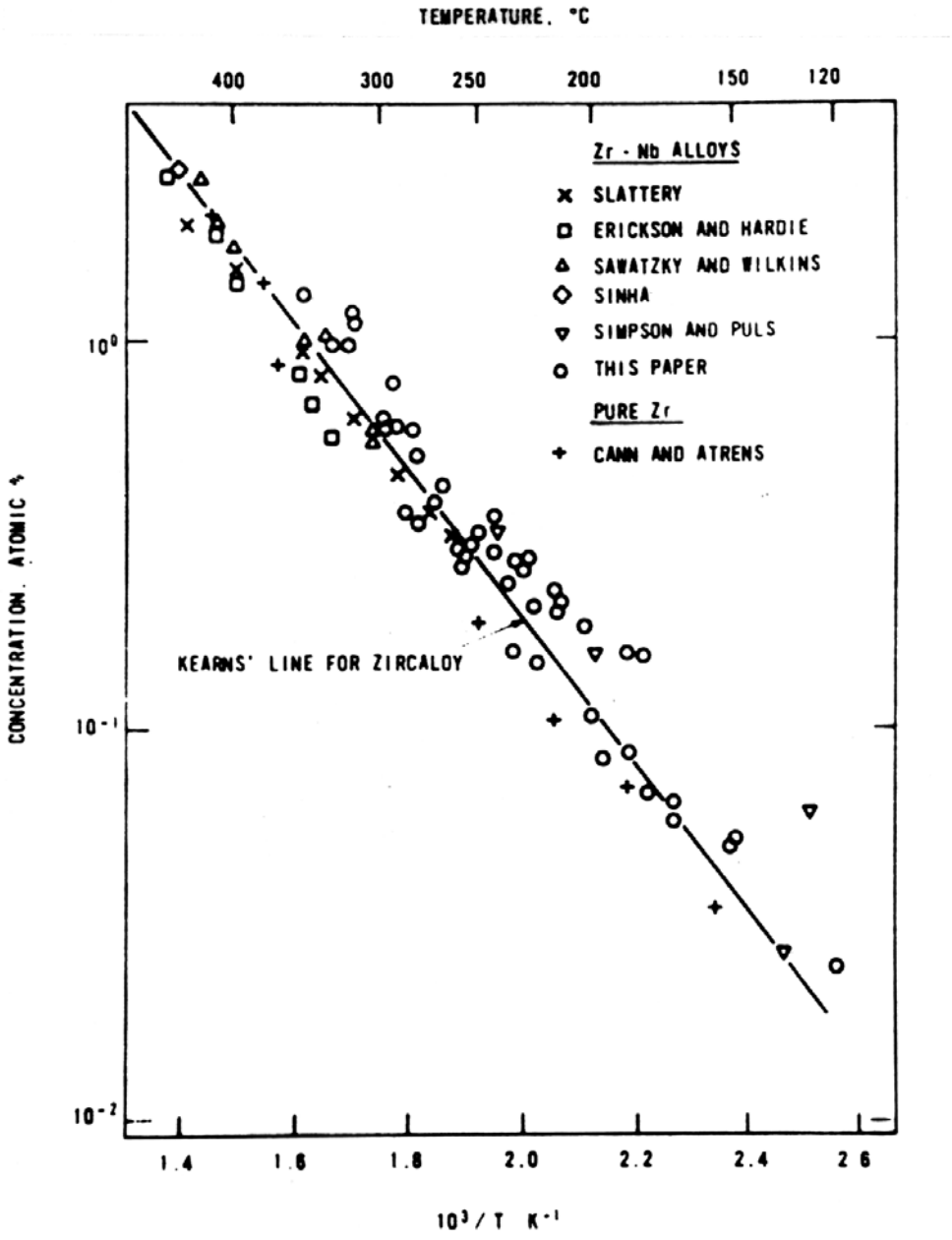

Figure 2-5: TSS for pure Zr

The dissolution and precipitation of hydrides is not instantaneous so that there is a hysteresis between the dissolution process (heating curve) and the precipitation process (cooling curve) resulting from the kinetics of dissolution and supersaturation on cooling respectively. It is usual to show the heating and cooling curves separately in the recent literature *Ref. 6*, and small differences in these curves resulting from alloying additions, fabrication variables (e.g. cold-working) *Ref. 7* and irradiation *Ref. 8* have been observed. Examples of these effects are shown in Figure 2-6 and Figure 2-7 and Figure 2-8.

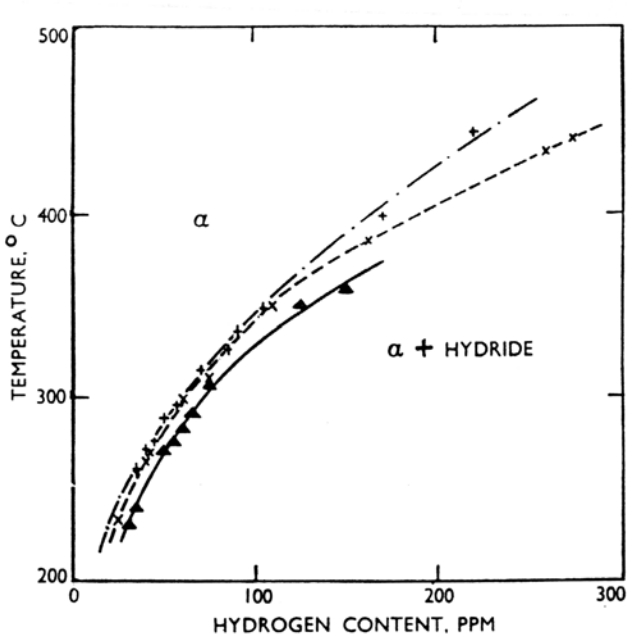

(a)

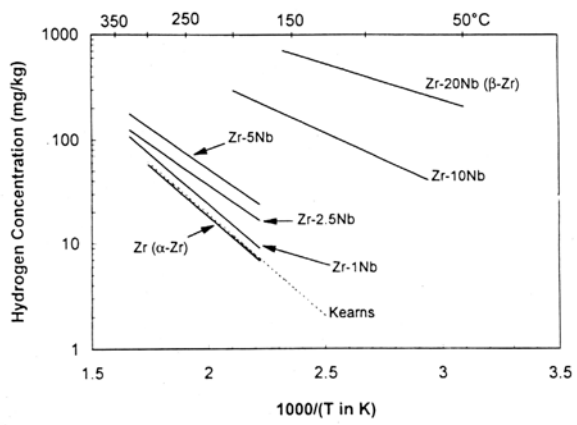

(b)

Figure 2-6: H solubility differences between Zr-alloys, (a) (▲) Zry-2, (X) Zry-4, (+) Zr2.5Nb; (b) TSS_d lines for hydrogen in Zr-Nb specimens with different Nb concentrations annealed at 1123K for 1 h. The lines for α-Zr and annealed Zr-20Nb (β-Zr) as well as the Kearn's line for unalloyed Zr are included for comparision

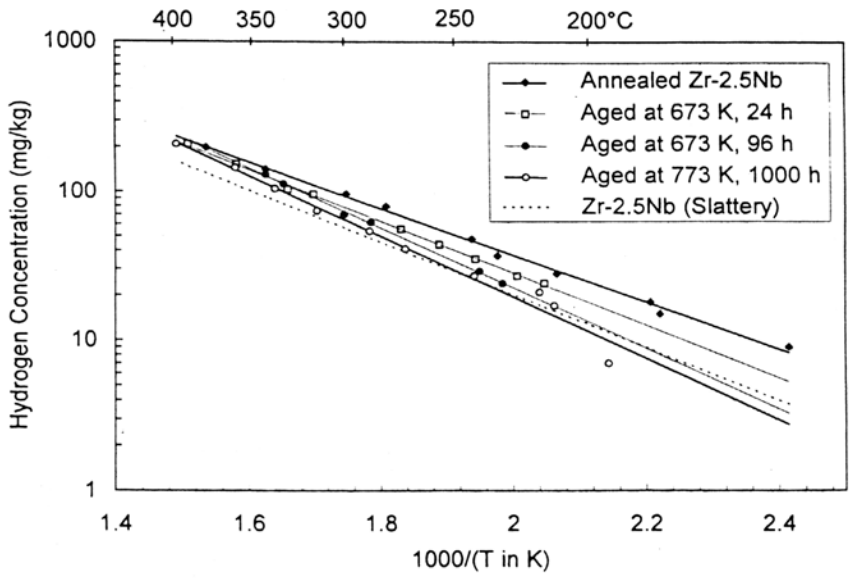

Figure 2-7: Effect of fabrication variables on H solubility; TSS_d for hydrogen in Zr2.5Nb annealed at 1123 K for 1 h (solid diamonds), aged at 673 K for 24 h (open squares) and for 96 h (solid circles) and aged at 773K for 1000 h (open circles). The solid lines are best fits to the data

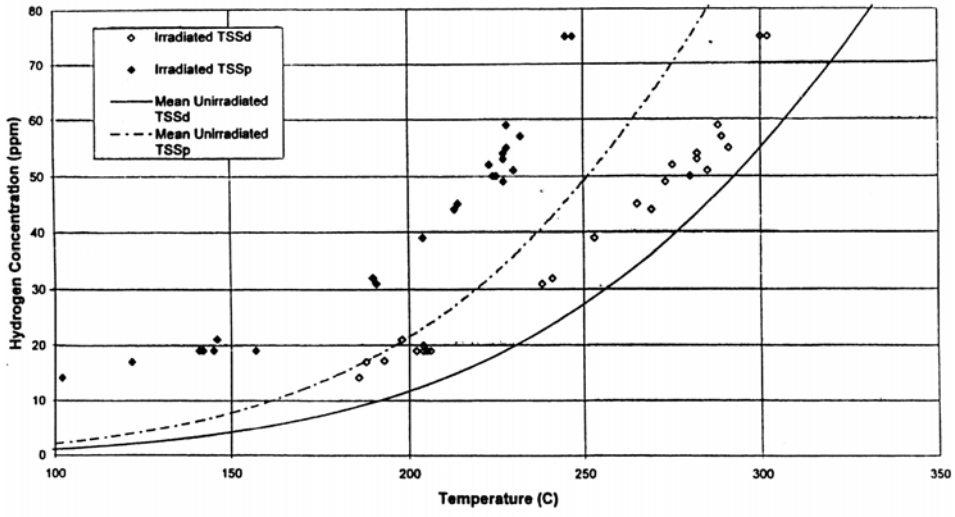

Figure 2-8: Effect of irradiation on TSS

The relatively slow kinetics of the hydride dissolution and precipitation processes are evident when the Differential Scanning Calorimetric (DSC) technique *Ref. 9* is used to measure the hydrogen content of a zirconium alloy specimen Figure 2-9.

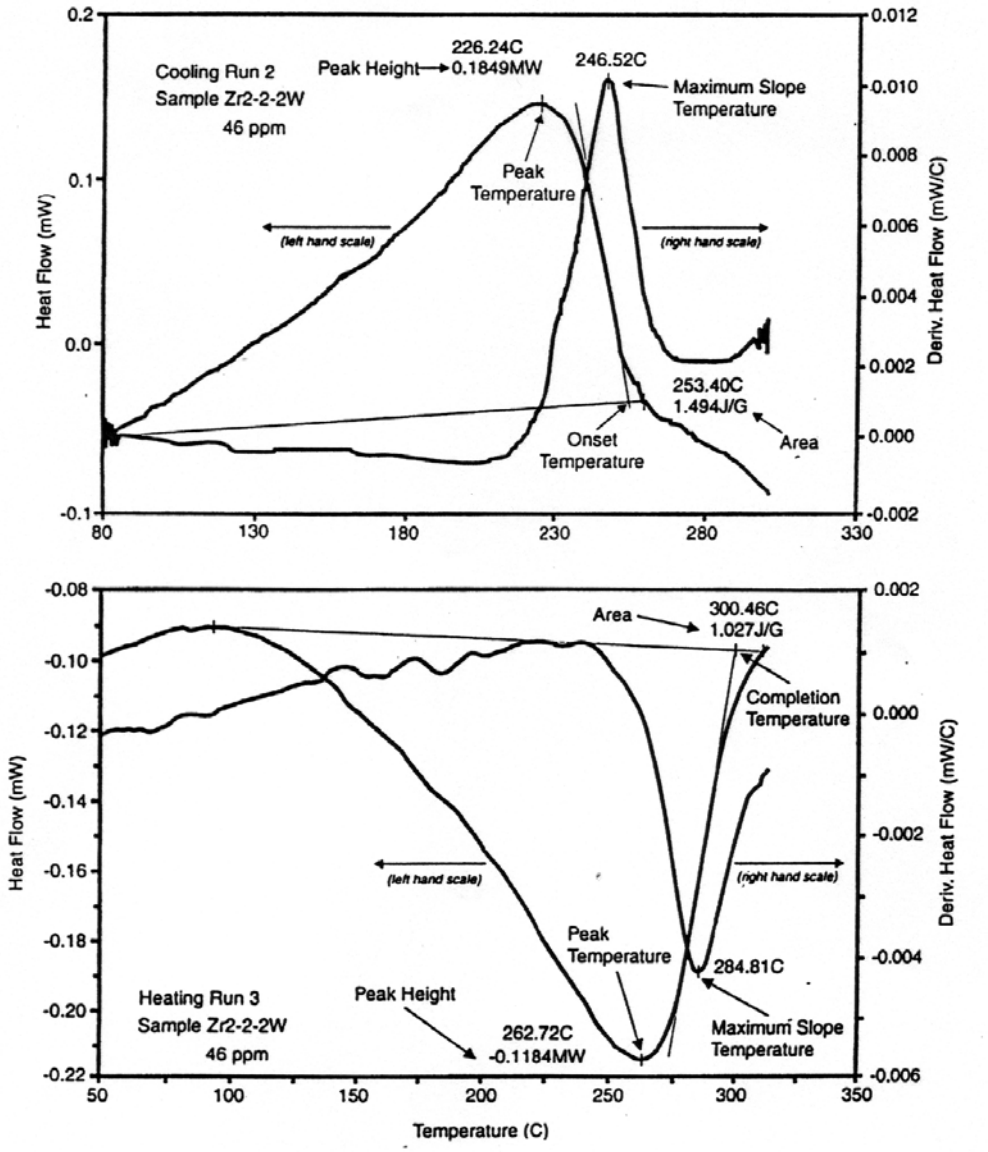

Figure 2-9: (b) Heating and (a) cooling curves from DSC measurement of same Zry-2 specimen

There remains some ambiguity as to which point on the curve represents the true solubility temperature. Is it, for instance, the temperature at which all the hydride has dissolved, or the temperature at which the maximum hydride dissolution rate occurs?

Hydrogen in solution in the α–Zr lattice occupies the tetrahedral interstices in the hexagonal α–Zr unit cell *Ref. 10* and causes a small dilation of the lattice. As a result of this, hydrogen shows a tendency to segregate to regions, such as the cores of dislocations, where the crystal lattice is already dilated *Ref. 11*. Because of this effect, hydrogen in solution in zirconium will migrate up a stress gradient (i.e. towards the region where the lattice is dilated by the elastic stress). Whether or not there is an effect of stress on the hydrogen solubility in Zr-alloys is determined by the difference between the lattice dilation caused by the hydrogen atoms in solution and the lattice dilation resulting from the formation of a second-phase hydride. These dilations can be described by the partial molar volumes of hydrogen in solution (V^h_H) and hydrogen in the appropriate hydride phase (V^h_{Hyd}) - usually δ–$ZrH_{1.66}$ - respectively. Despite claims to the contrary *Ref. 12* measurements of these partial molar volumes have shown them to be nearly equal, so that the effect of external stress on TSS is negligibly small *Ref. 13*, typically less than one centigrade degree. These effects on stress on hydrogen migration are critical to the mechanism of Delayed Hydride Cracking in Zr alloys.

2.1.2 Hydrogen diffusion

Although hydrogen has very limited solubility in α-Zr especially at low temperatures, it has high diffusivity. Measurements of hydrogen diffusion coefficients were made early *Ref. 14-16.* Hydrogen will diffuse down a concentration or temperature gradient, but diffuses up a stress gradient. The diffusivity of hydrogen in α-Zr is given by the equation

$$J = -D\left(\nabla c + \frac{Q^* \cdot c}{RT^2}\nabla T\right)$$

where J is the flux of hydrogen atoms in the metal

D is the diffusivity given by $D = 2.17 \times 10^{-3} \exp(-8380/RT)$

C is the local concentration

Q* is the heat of transport (about 6 Kcal/mol.)

and ∇ is the rate of change (i.e. gradient) of C or T

Although this equation predicts rapid migration down both concentration and temperature gradients, this is only true for temperature gradients if the solubility is exceeded at the cold end of the gradient and hydrides are precipitated there. Provided all hydrogen remains in solution throughout the material, the increase in heat of solution *Table 2-1* with decreasing temperature leads to a small increase in hydrogen concentration at the cold side of the temperature gradient when equilibrium is achieved. The same is true of the hydrogen concentration profile in a stress gradient, there is only a small increase in hydrogen concentration in the high stress region provided TSS is not exceeded in this region. Since there is no effect of stress on TSS (see above) it is only when hydrogen concentrations are close to TSS that continuous precipitation in a region of high triaxial stress (e.g. at a notch) can lead to DHC.

Hydrogen diffusion coefficients show a sharp increase at the α/β phase change, since diffusivity (and solubility) are much higher in the bcc β–Zr phase Figure 2-10. This has important consequences for alloys with additions that stabilise the β–Zr phase at room temperature (e.g. Zr-2.5%Nb).

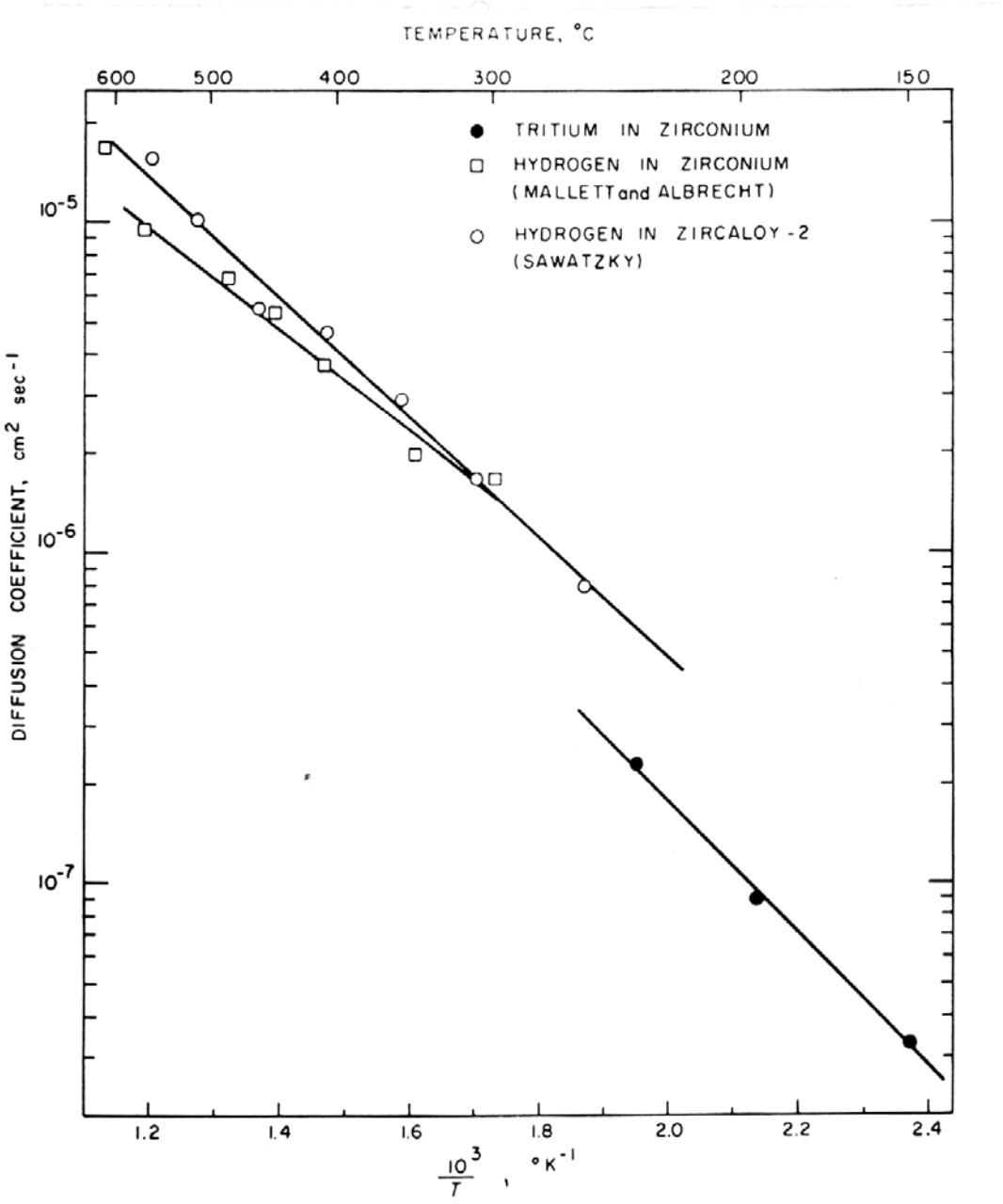

Figure 2-10: H diffusivity in the α–Zr phase

Fabrication of such alloys leads to a two-phase product, and deformation during tube fabrication can lead to filaments of β–Zr that are continuous along the elongated grain boundaries of such alloys. The effective diffusivity for hydrogen in these alloys is then a composite of the diffusivities of hydrogen in the α–and β–phases at the same temperature, and is determined by the relative partial cross-sections of the two phases in the direction of diffusion, and the continuity of the phase with the high H diffusion coefficient (β–Zr). These effects have been extensively studied because of their importance to DHC crack velocities in such alloys *Ref. 17.*

Hydrogen diffuses interstitially in the α–Zr lattice, and since the c/a ratio of α–Zr (1.593) is not equal to that of a perfect hexagonal close packed lattice (1.63) the diffusion coefficients of interstitial diffusers are expected to differ between the basal plane and prism plane orientations, Figure 2-11. Thus, the texture of the Zr alloy component can have a small effect on the hydrogen diffusivity in different directions *Ref. 18.*

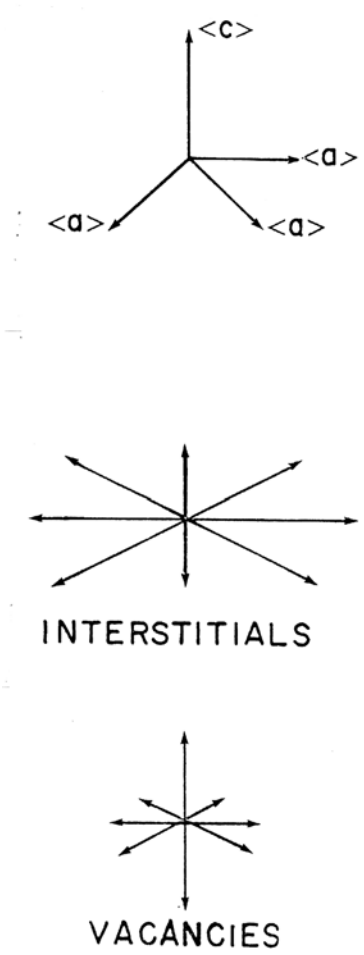

Figure 2-11: Directional dependence of diffusion in β–Zr

2.1.3 Nucleation and growth of hydrides

The nucleation of zirconium hydride precipitates in α–Zr is <u>not</u> an example of "homogeneous nucleation and precipitation". Even in pure α–Zr the hydrides nucleate on prefered crystal planes *Ref. 19.* There are several such orientations of which $(10\bar{1}7)$ is that most commonly observed. Although the partial molar volumes of hydrogen in solution and hydrogen in δ–$ZrH_{1.66}$ are the same for all practical purposes, so that there is no net volume change on precipitation, the previously distributed lattice dilations due to hydrogen in tetrahedral interstices must be collected into the volume being converted to hydride, while the rest of the lattice relaxes. This results in the generation of dislocation loops around the hydride platelet as they form Figure 2-12, *Ref. 20.*

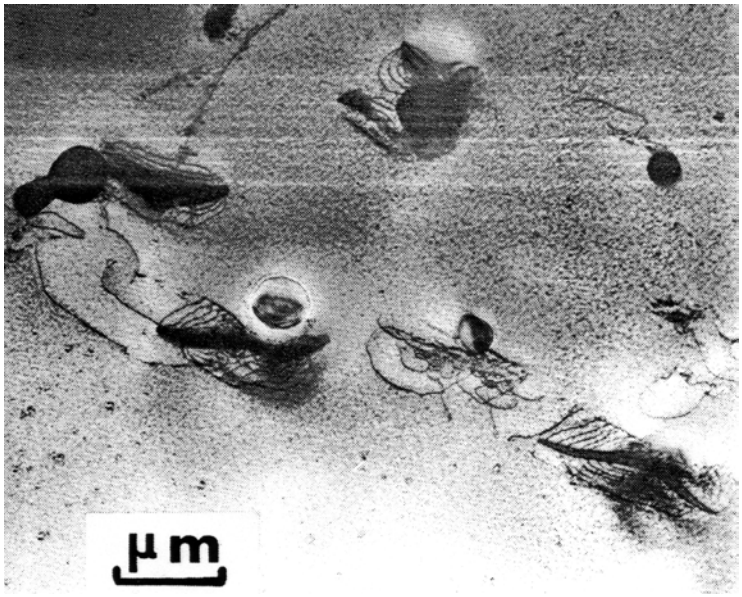

Figure 2-12: Hydride nucleation at intermetallic particles in Zry-2

In polycrystalline materials the grain boundaries become the preferred sites for the hydride nucleation and growth and intra-granular precipitation is only prominent for large grain sizes or rapid cooling rates. When the grain shapes are not equiaxed then the situation becomes more complicated and some grain boundaries may be preferred over others. There can be, thus, a whole hierarchy of nucleation sites, and when cooling rates are slow, so that hydrogen can diffuse over large distances prior to precipitation, the situation can lead to long stringers of hydride made up of many small aligned hydride platelet, Figure 2-13, *Ref. 21.*

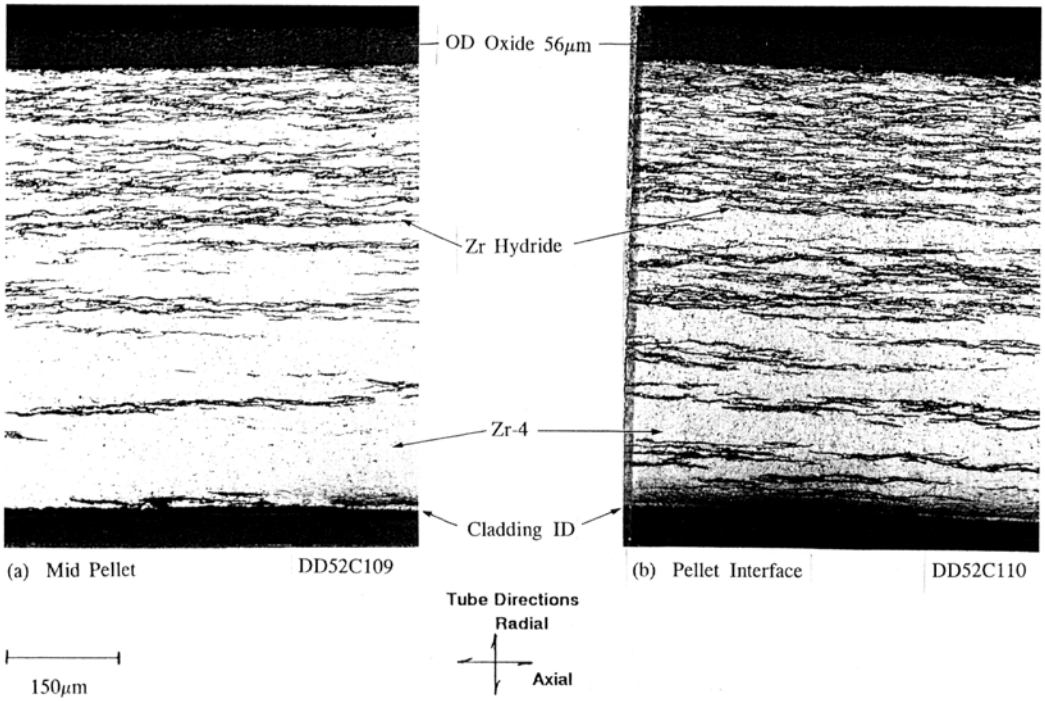

Figure 2-13: Typical fuel cladding hydride distributions

It is very difficult to prevent hydride nucleation by rapid quenching. However, it can be done provided the specimen temperature is kept low to prevent nucleation subsequently. Hydrogen diffusion is so rapid that hydrides will nucleate even in rapidly quenched specimens at temperatures only a little above room temperature. The act of mounting a quenched specimen for examination in so-called "cold-setting" epoxy can be enough to cause hydrides to nucleate *Ref. 22.* 1hr at 100°C is sufficient to produce very small hydrides.

The growth of long hydride stringers gives the appearance (when specimens are metallographically polished and etched for examination) of a continuous hydride structure. However, this is a function of the etching process which broadens the apparent hydride by producing an array of etch pits. In the transmission electron microscope these apparently continuous stringers can be resolved into an alignment of small individual hydride platelets. Thus, it appears that the "hydrides" grow longer by the successive nucleation of small platelet adjacent to each other. This may arise because of the dislocation loops punched out by the first small initial platelet Figure 2-14, *Ref. 20.* There is evidence that hydrogen atmospheres develop in the cores of dislocations because the lattice is dilated in this region *Ref. 11* and *Ref. 23.* This local concentration of hydrogen may then provide the site for the nucleation of another small hydride platelet adjacent to the first. The generation of more dislocation loops would then allow for a continuous succession of small aligned hydrides to form. This would result in the appearance of an apparently continuous hydride precipitate when a polished section through the array was etched.

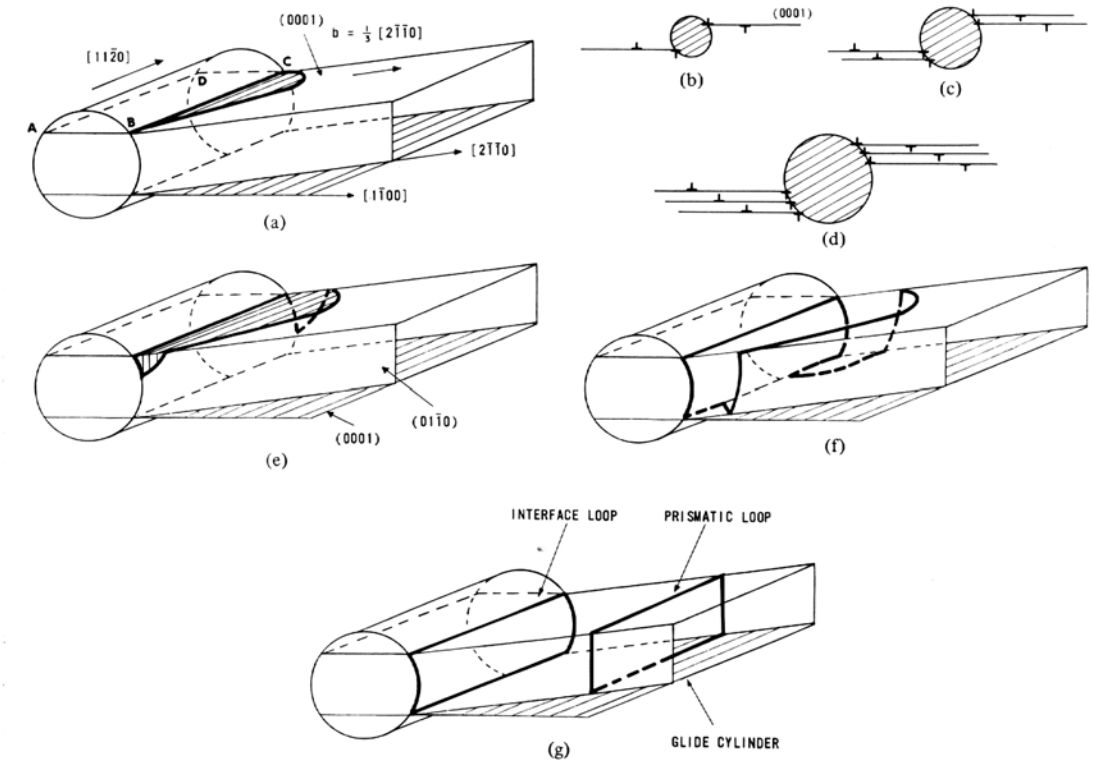

Figure 2-14: Dislocation generation during hydride precipitation: (a) shear loop formation, (b)-(d) projection along $[11\bar{2}0]$ showing effect of growth, (e) and (f) cross slip, (g) prismatic loop formation.

2.1.4 Mechnical properties of hydrides

Due to the low hydrogen solubility in the zirconium matrix, being about 100 wtppm at reactor operating temperature, most of the hydrogen released through the corrosion process between steam/water and the zirconium alloy may precipitate out as zirconium hydrides. This hydride phase is normally brittle and if the zirconium alloy contains sufficient amounts of zirconium hydrides, the mechanical performance of the metal may be deteriorated. Since the mechanical performance is to a large extent impacted by the stress state and strain rate, it is imperative to take these parameters into account when test method and specimen geometry is selected to simulate a specific in-reactor situation. One of the most important material parameters to be assesses in mechanical tests is the material ductility, i.e., the material possibility to plastically deform without failing. To generate conservative ductility data in the mechanical tests, researchers uses environmental conditions (strain rate, temperature, etc.) and a specimen geometry that enhances the brittle behaviour of the material. Normally, increased strain rate and lowering of the test temperature will reduce the material ductility. Also, introducing a defect such as a sharp notch (fracture mechanic tests) and by increasing the specimen dimensions will result in a more brittle behaviour of the material.

The hydrides may impact the zirconium alloy during shut-down, normal and off-normal reactor operation as well as during intermediate storage. During refuelling shut-down the zirconium alloy temperature is about 30-40°C, while the corresponding temperature is about 290-400°C during normal reactor operation. Considering, these two cases, there are two different situations to be taken into account. First during shut-down, the fuel assembly may be damaged during handling. The fuel assembly may e.g., hit another component and during such a case, the strain rate is very high. To correctly evaluate the impact of hydrides in zirconium alloys in such a case, the strain rate must be high as is the case e.g., during Charpy-V impact testing at lower temperatures. During normal reactor operation of non-failed fuel, the limiting situation is a power transient that may result in fuel cladding deformations. Relevant mechanical tests for such a situation are tests with lower strain rates at higher temperatures. Up to last year some researchers believed that tendency for BWR failed fuel degradation by forming long axial cracks could be measured by fracture mechanic tests. It appears now that this is not the case since the fracture mechanism in the formation of these long axial cracks is very different from that existing during fracture mechanics tests. The former mechanism is named *Delayed Hydride Cracking, DHC.* Fracture mechanics tests are still however relevant to assess fuel cladding performance during a *Reactivity Initiated Accident, RIA.*

In the following some relevant mechanical test data of hydrided materials is provided.

Tensile tests at room temperature show that the Zircaloy material ductility decreases with increased hydrogen content, Figure 2-15. The tensile strength appears to be constant for Zry-2 materials with up to about 500 wtppm of hydrogen, Figure 2-16. Based upon these early results, *Whitmarsh, Ref. 25,* suggested a maximum allowable hydrogen content in Zry-2 of 500 wtppm. This maximum hydrogen content is today used by some fuel vendors as a design limit of their zirconium alloy components. *Lin and Hamasaki, 1979, Ref. 26* on the other hand suggested a maximum hydrogen content of 300 wtppm also based upon tensile tests performed at room temperature, Figure 2-17.

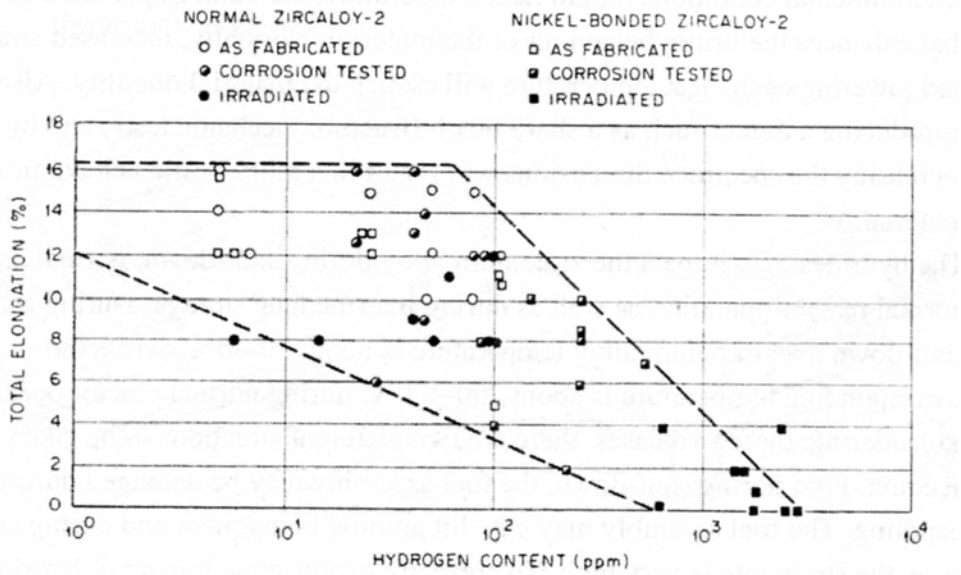

Figure 2-15: Impact of hydrogen content on Zry-2 ductility at room temperature, Yeniscavich et al., 1958, Ref. 24.

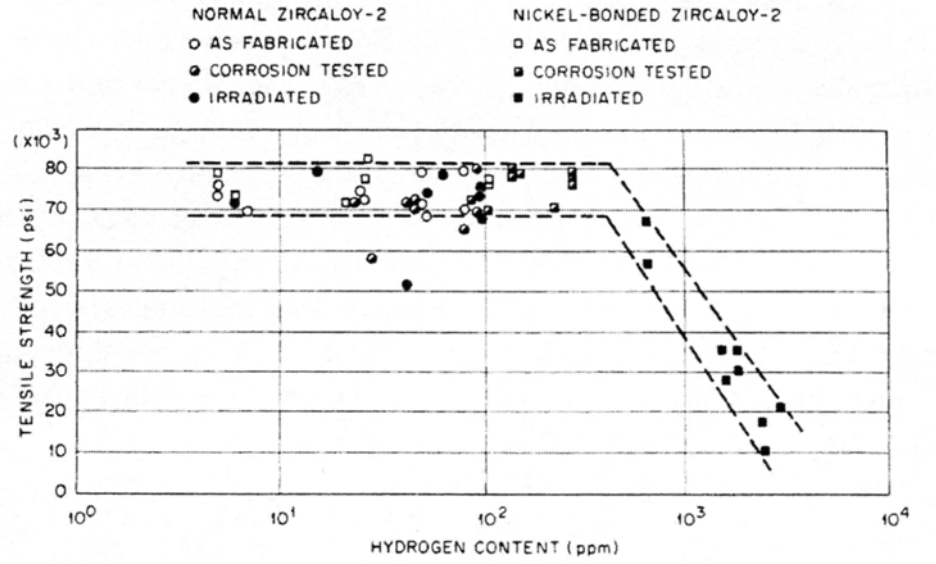

Figure 2-16: Impact of hydrogen content on Zry-2 tensile strength at room temperature, Yeniscavich et al., 1958, Ref. 24.

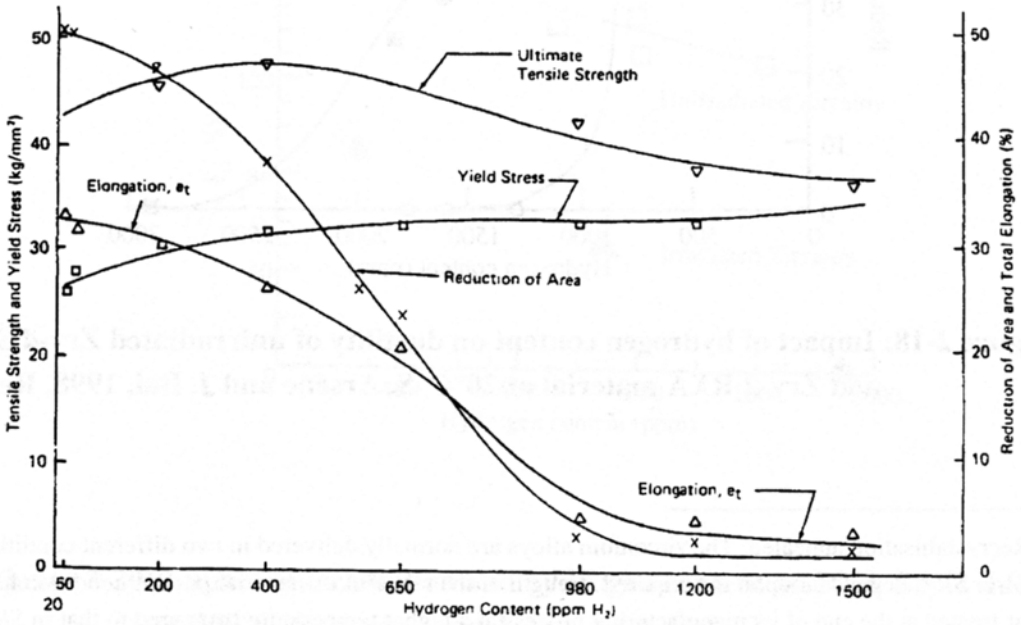

Figure 2-17: Impact of hydrogen content on mechanical properties of Zry-4 at room temperature, Lin and Hamasaki, 1979, Ref. 26.

The temperature has a dramatic impact on ductility of hydrided zirconium alloys Figure 2-18, Figure 2-19 and, Figure 2-20. Tensile tests were done on prehydrided nonirradiated and irradiated Zry-2 and –4 in *RXA*[1] and *SRA* conditions. It is clear from these figures that increased hydrogen content reduces the plasticity of the materials, manifested by a *reduction in area*[2] and in ductility. In Figure 2-18 and Figure 2-19 one can see that increasing the temperature will maintain a ductile material even with increased hydrogen contents. At 300°C up to about 2000 wtppm of hydrogen may exist in the unirradiated material without significantly impacting its ductility. Figure 2-20 does however show that the impact of hydrogen on ductility is somewhat stronger in irradiated than in unirradiated materials.

[1] Recrystallisation annealed. The zirconium alloys are normally delivered in two different conditions , *RXA* or *SRA*, dependant upon the required strength of the material. A material in *RXA* condition has been heat-treated at the end of its manufacturing process at a higher temperature compared to that in *SRA* condition. The higher temperature of the *RXA* material will reduce the material strength and increase its ductility.

[2] There are different measures of ductility, one being *area reduction* that is the decrease in area cross section at the failure location from the initial cross section value. This means that increasing values of area reduction indicate larger ductility values.

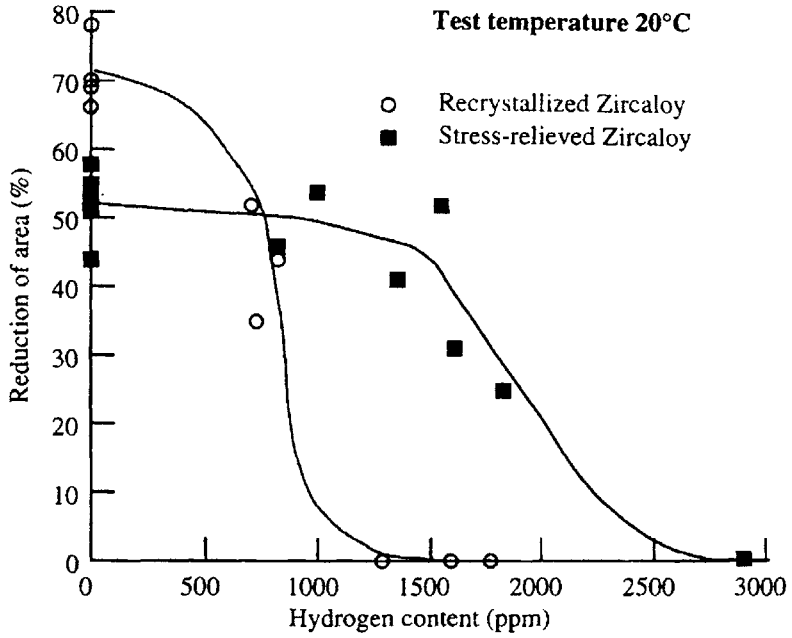

Figure 2-18: Impact of hydrogen content on ductility of unirradiated Zry-4 SRA and Zry-2 RXA material at 20°C, S. Arséne and J. Bai, 1998, Ref. 27.

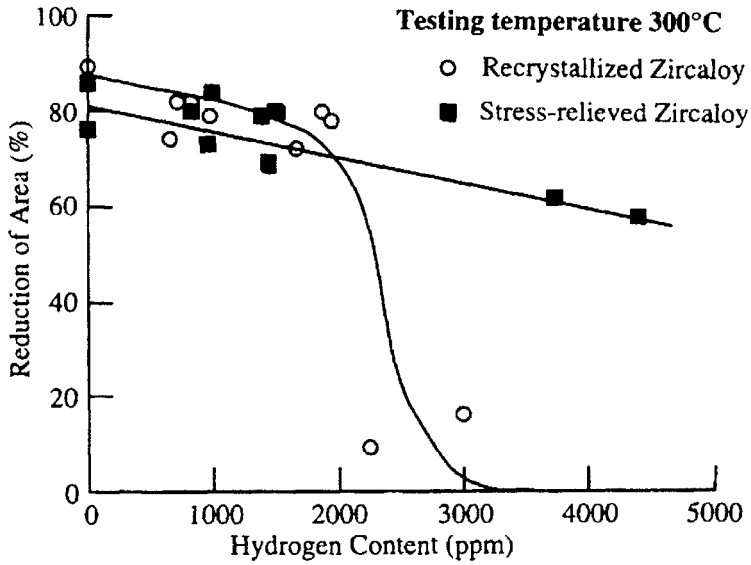

Figure 2-19: Impact of hydrogen content on ductility of unirradiated Zry-4 SRA and Zry-2 RXA material at 300°C, S. Arséne and J. Bai, 1998, Ref. 27.

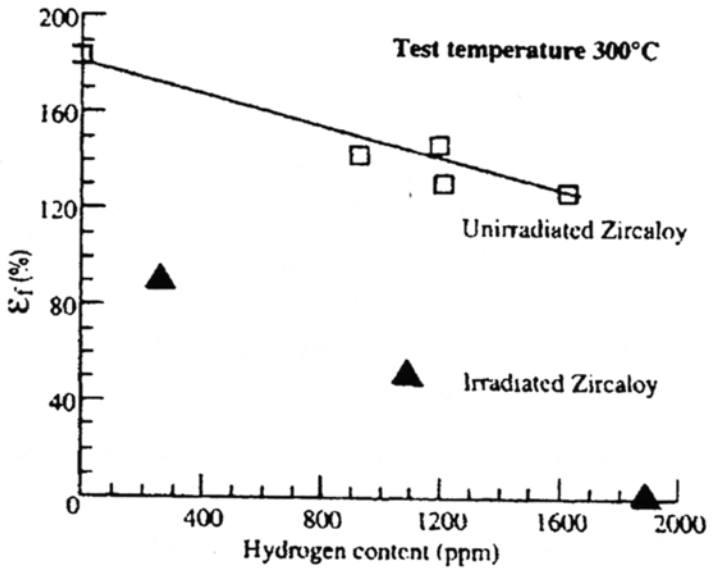

Figure 2-20: Impact of irradiation and hydrogen content on RXA Zry-2 ductility at 300°C, S. Arséne and J. Bai, 1998, Ref. 27.

The reason for the increased ductility at higher temperature is related to the fact that the zirconium hydride alters fracture properties from being brittle at low temperatures to becoming ductile at higher temperatures, Figure 2-21.

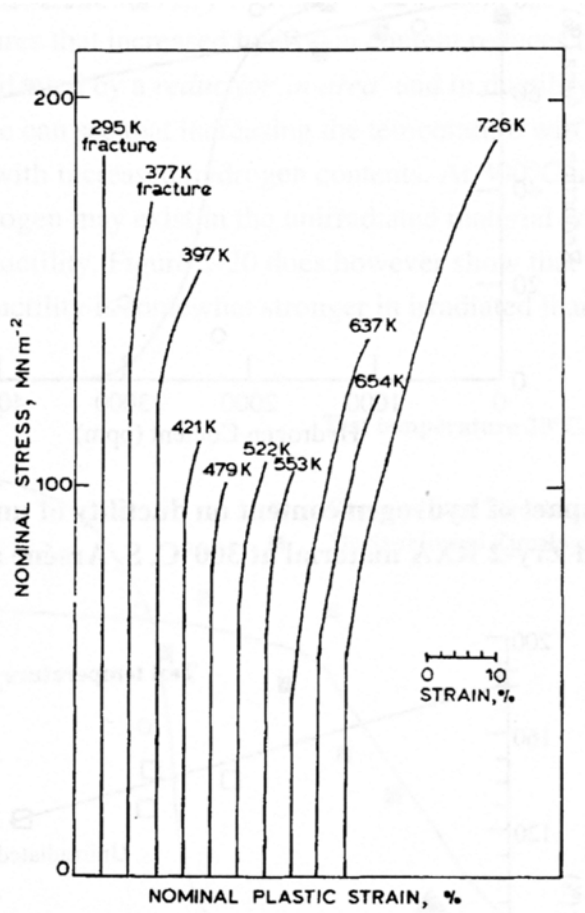

Figure 2-21: Typical stress – strain curves for stoichometric hydride, δ-$ZrH_{1,66}$, *Northwood och Kosashi, 1983, Ref. 28.*

The results from Charpy-V impact testing of Zry-2 with varying hydrogen concentrations are shown in Figure 2-22. It is clear that the Zry-2 material becomes more brittle if the hydrogen has precipitated out (compare the two curves for 38 ppm hydrogen in solution and as precipitated hydrides).

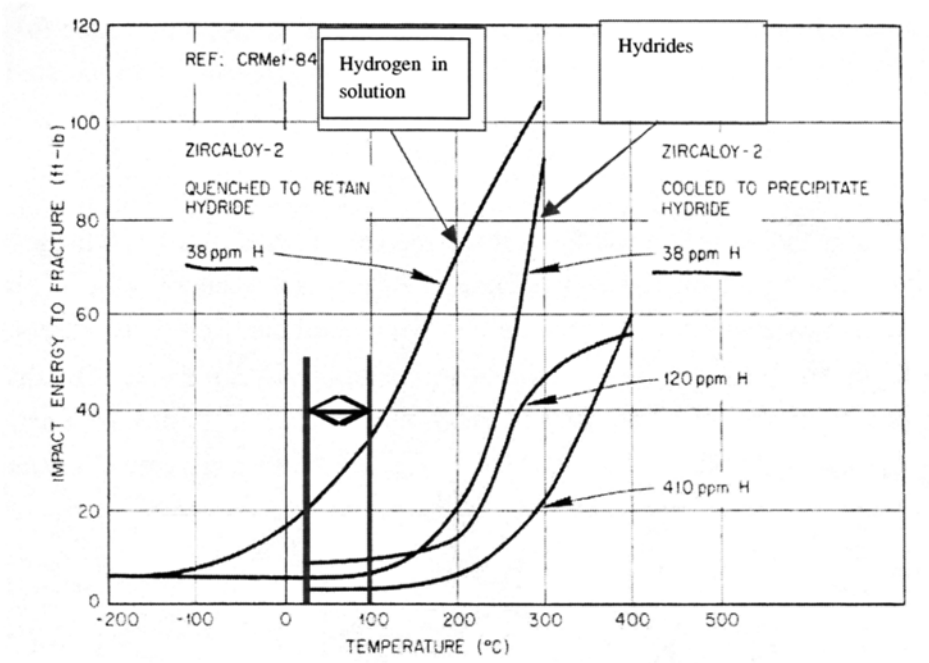

Figure 2-22: Impact of hydrogen on impact ductility of Zry-2, modified figure according to Ref. 25.

Hot cell examination was done on two failed nonliner GE rods that behaved very differently in-reactor. The fuel claddings were manufactured at different times. The fuel cladding of a more recent manufacturing date had a defect that had developed into an axial split 31 cm in length while the fuel cladding with a older manufacturing date did not degrade, *Ref. 29.* TEM examination of non-irradiated archive material of the two different cladding lots showed a dramatic difference in second phase particle size distribution, related to different manufacturing processes.

Edsinger et al., 1999, developed a special technique, referred as the Vallecitos Embedded Charpy, *VEC*, to measure the fracture properties of thin-walled Zircaloy material, Figure 2-23. The specimen is inserted into the four internal pieces of the *VEC* fixture to form a bend bar with the same dimensions as a Charpy specimen. *Edsinger et al., 1999, Ref. 31,* reports that the *VEC* is treated analytically, as a standard three point bend fracture toughness specimen and that the calculation of the K and J [3]is based on the dimensions of the Zircaloy specimen. The authors state that all specimens were fatigue precracked to desired crack depth to specimen width ratio. The fracture toughness was calculated as:

[3] For thin specimens such as e.g. cladding tubes, the plastic zone ahead of the crack tip becomes large in relation to the specimen dimensions. A plane strain situation does not exist in such a case, but rather a plane stress condition. If plane stress exists a J value is calculated as a measure of the maximum stress level ahead of the crack tip and when this value reaches J_C, crack propagation occurs.

$$J = \frac{\alpha E_M}{bB} \qquad \textbf{Eq. 2-1}$$

where E_M is the absorbed energy at initiation (elastic and plastic), b is the length of the remaining ligament, i.e., (specimen length – crack length W-a, B is the specimen thickness and α is the geometry dependant constant (Edsinger et al., 2000). The fracture toughness was then calculated from Eq. 1 assuming that crack initiation coincided with the point of maximum load, i.e. J_{max} for both elastic and elastic-plastic behaviour, and the value of J_{max} was converted to an equivalent value of K.

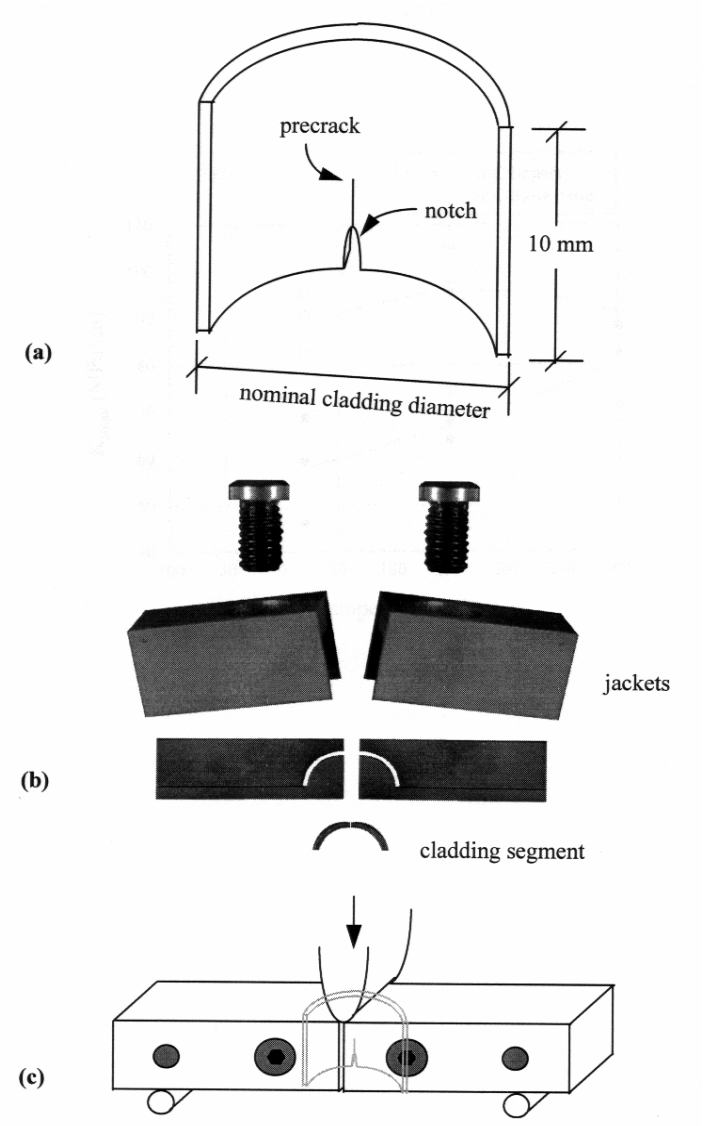

Figure 2-23: (a) cladding specimen, (b) fixture assembly and (c) loading for VEC testing, Edsinger et al., 2000, Ref. 30.

The *VEC* test was used to assess the fracture toughness of the GE irradiated materials with different initial second phase particle size distributions that behaved very differently regarding secondary degradation resistance of failed BWR fuel. The fuel rod with initially larger second phase particles did not degrade while that with initially small precipitates did form a long axial crack. *The results indicate that the VEC test cannot differentiate between the two materials,* Figure 2-24*. For irradiated specimens with about 400 wtppm of hydrogen, the fracture toughness is the same for the two materials. Thus, the VEC test does not produce the same failure mechanisms at that in the BWR. If that would have been the case, one would have expected that the material that did not degrade would show much higher fracture toughness value compared to the material that did degrade.* Figure 2-24 *also show that increasing hydrogen content decreases fracture toughness.*

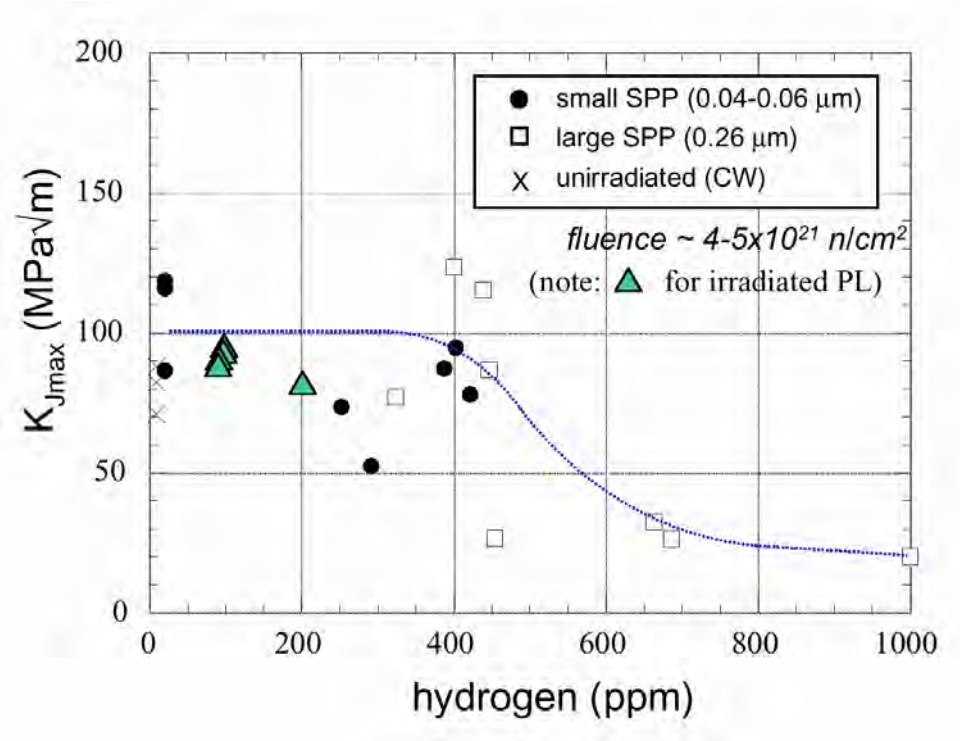

Figure 2-24: Fracture toughness results from the VEC and PL techniques as a function of Hydrogen. Data presented by Grigoriev by PL-testing is also provided as comparision, Edsinger, 2000, Ref. 30.

Summarising all the data it is obvious that increasing hydride content in the zirconium alloy material will increase the material brittleness in mechanical tests. However, increasing temperature will dramatically increase the ductility of the material and restore the material ductility even if it contains significant amounts of hydrides. Out-of-pile mechanical tests are often used to investigate the material mechanical performance in-pile. Since the temperature has such a big impact on ductility, it is crucial to apply a test temperature that is comparable to the temperature that exists in-pile or otherwise the test may be too conservative.

3 HYDROGEN PICKUP MECHANISM

Hydrogen gas is absorbed very rapidly by zirconium alloys if an oxide free surface *Ref. 32* is produced, however. Even a very thin layer of oxide interposes an almost impermeable barrier. The critical question to be addressed by any hydrogen absorption hypothesis for material bearing an oxide film is how do the hydrogen atoms penetrate this oxide? There will always be an oxide layer present whenever zirconium alloys are exposed to an atmosphere containing oxygen in any form at temperatures close to water-reactor coolant temperatures. Thus, hypotheses about hydrogen absorption during aqueous corrosion are inevitably closely related to hypotheses about the nature of the oxide formed.

Early views of the corrosion process pictured the initial formation of an imperious barrier type oxide controlled by the diffusion of oxygen vacancies through it (pre-transition oxidation). At some point this barrier oxide started to breakdown and the initially cubic/parabolic kinetic rate law changed to an approximately linear (post-transition oxidation) rate law. During this period a residual impermeable barrier oxide of approximately constant thickness was considered to control the corrosion rate near to the oxide/metal interface. Thus, for hydrogen to be absorbed by the metal during the corrosion process it had to be able to diffuse through some, or all, of the zirconium oxide film. The cathodic half-cell reaction of the oxidation process,

$$2e^{-} + \otimes^{\circ} + H_2O \rightarrow O^{2-} + 2H^{\circ}$$

where $\otimes^{\circ}$ is an oxygen vacancy in the ZrO_2 lattice,

O^{2-} is an oxygen ion in the ZrO_2 lattice, and

H° is an hydrogen atom,

was generally considered to take place at the environment side of any barrier oxide film present and the hydrogen atoms liberated by it were thought to diffuse through the impervious oxide barrier (not necessarily in this chemical form) in order to enter the metal. Some of them were expected to recombine to form hydrogen molecules and be released into the environment, thus giving rise to the "percentage hydrogen uptake" which was the ratio of the hydrogen entering the metal to the total hydrogen generated by the cathodic reaction *Ref. 33.* The anodic half-cell reaction is the one that causes the increase in the thickness of the oxide film. The two together comprise the total oxidation process.

$$Zr + 2H_2O \rightarrow ZrO_2 + 2H_2$$

The hydrogen uptake hypothesis thus required a diffusion coefficient for hydrogen (in some unspecified form) through ZrO_2. Attempts to measure such diffusion coefficients were generally flawed, for a variety of reasons *Ref. 34* so that no generally acceptable value for hydrogen diffusion in ZrO_2 is available.

Difficulties in pinning down a value for this diffusion coefficient, were paralleled by growing doubts about the extent of the impermeability of the so-called "barrier" oxide film at the oxide/metal interface Ref. 35. If this oxide had a small (but significant) number of flaws in it that could act as sites for easy flow of the cathodic current, then the cathodic process could be occurring at a few very localised sites and the hydrogen uptake process might not be uniform over the whole corroding surface Ref. 36, but could occur preferentially at regions where cathodic currents flowed most readily (e.g. welds or braze heat-affected zones). The hydrogen uptake mechanism would then look very different since there might be no barrier oxide at the sites of flaws (cracks?) in the generally still protective oxide film.

Mechanistically the answers to these questions of whether the "barrier" oxide is truly impervious to molecular species or contains a significant number of flaws, and whether these flaws represent local sites for the cathodic reaction to occur, still need unequivocal evidence. However, a number of observations can be explained if the oxides are invariably flawed, but cannot be if they are perfect barriers. The sites of these flaws have been variously considered to be small cracks in the oxide *Ref. 35* and *Ref. 36* or the sites of intermetallic particles *Ref. 37*.

In the following some recent data that is related to the hydrogen pickup mechanism are presented.

3.1 ZIRCALOY

A uniform and nodular corrosion and hydriding model for Zircaloy material was presented by *Rudling and Wikmark, 1999, Ref. 38*. In this work, a novel way of describing the processes were presented with corrosion and hydriding steps in parallell and in series. The inverse rate constant or reaction ”resistance”, designated *RR* were used in the model. These reaction resistances were not to be interpreted as electrical resistances. Each reaction was related to a specific corrosion/hydriding step. The analogy with common electrical resistances was that the reaction resistance in the series that had the highest value or the shunting parallel reaction resistance having the lowest reaction resistance, i.e., the rate limiting step, would govern the overall corrosion rate. The hydrogen pickup, that is a product of the corrosion rate and the hydrogen pickup fraction is modelled according to Figure 3-1. Increasing the oxidation potential in the coolant would increase the reaction resistance $RR_{H,\text{ water chemistry}}$ resulting in a lower hydrogen pickup fraction if the overall hydrogen pickup process was limited by this reaction resistance. Also for hydrogen pickup the authors suggested that the barrier layer played an important role. The hydrogen atoms might take two routes into the metal, either through the second phase particles, SPPs, (at normal barrier layers) or directly through the barrier layer (when this was very thin). The hydrogen transport through the barrier layer was modelled by the reaction resistance of $RR_{\text{H, barrier layer}}$. It was inferred that initially, before the transition, the hydrogen pickup fraction would be very large due to a very thin barrier layer. The increasing barrier layer thickness during pre-transition growth would dramatically increase the $RR_{\text{H, init. barrier}}$ value. This would result in a dramatic decrease in the hydrogen pickup fraction during the course of oxidation in the pre-transition regime and a shift from hydrogen ingress through the barrier layer through the SPPs where the latter process was modelled by $RR_{\text{H, init. SPP}}$.

It is well-known that Zry-2 has a higher pickup fraction compared to Zry-4 and the largest microstructural difference between these two different materials is that Zry-2 contains both nickel-and chromium bearing particles while Zry-4 only contains the latter type, e.g. *Ref. 39*. Thus, it would seem that the reason for the larger hydrogen pickup fraction in Zry-2 is related to the nickel-bearing particles. In Rudling and Wikmarks model, $RR_{\text{H, SPP}}$ relates to the impact of SPP on hydrogen pickup fraction. The authors further suggest that e.g. a nickel-containing SPP results in a smaller reaction resistance than chromium-particles thus increasing the hydrogen pickup fraction.

4 REDISTRIBUTION AND REORIENTATION OF HYDRIDES IN ZIRCONIUM ALLOYS

There are three principal forces that redistribute hydrides in zirconium alloys. These are temperature gradients; stress gradients and the hysteresis in solubility between the "heating" and "cooling" curves. Apart from the localisation of hydrides on a scale comparable with the grain size resulting from various preferential sites for precipitation, the hydrogen distribution in an isothermal specimen is expected to be uniform when averaged over the bulk of the specimen *Ref 19* and *Ref. 43.* This is only true provided local hydrogen absorption rates are low compared with the rate of equilibration of hydrogen in the matrix. If local absorption rates are high, such as during the pre-hydriding of specimens in high temperature hydrogen gas, then the absorption rate can exceed the equilibration rate and a solid hydride blister forms at the site of the rapid hydrogen absorption *Ref. 44.* Solid hydride layers are most readily formed by low temperature absorption mechanisms that can give high absorption rates at temperatures where diffusion away from the surface is slow (e.g. cathodic hydriding at room temperature) *Ref. 33* and *Ref. 45.* For reactor components (such as guide tubes), however, except in exceptional circumstances, the hydride distribution through the tube wall at any elevation should be uniform.

For fuel cladding, or any other situation involving a heat flux, the increasing heat of solution with decreasing temperature causes the concentration of hydrogen in solution to be slightly higher at the cold (outer) surface of the cladding Figure 4-1, *Ref. 46.*

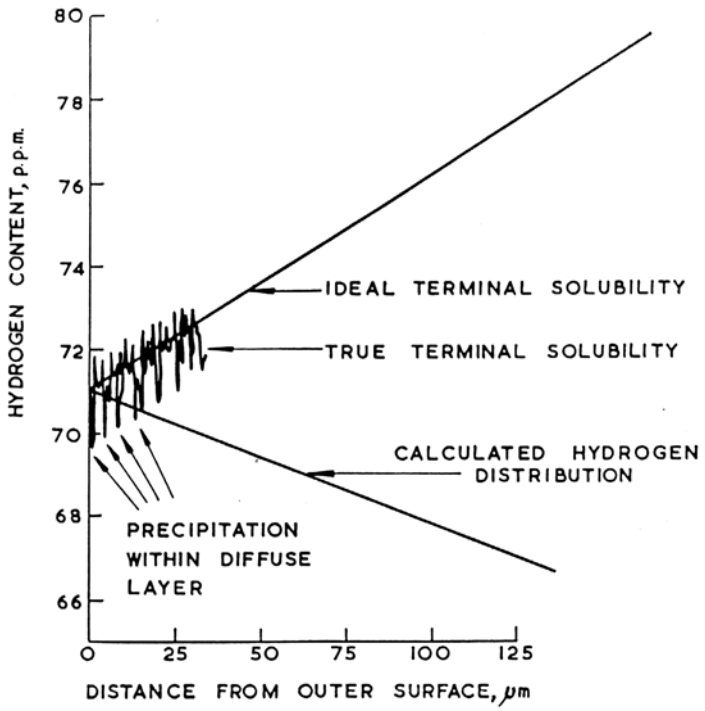

Figure 4-1: Development of diffuse α+δ region in fuel cladding

Under these conditions TSS will be reached first at the cold surface, and all the subsequent hydrogen absorbed should precipitate as a solid layer at this surface. However, the presence of preferential sites for precipitation (equivalent to TSS varying with position) results in a diffuse two-phase ($\alpha+\delta$) region being formed at the cold surface. If the temperature is rendered more severe locally as a result of patches of spalled oxide and/or pellet/pellet gaps then a solid hydride blister (or lens) may form at this site Figure 4-2 *Ref. 47* and *Ref. 48.*

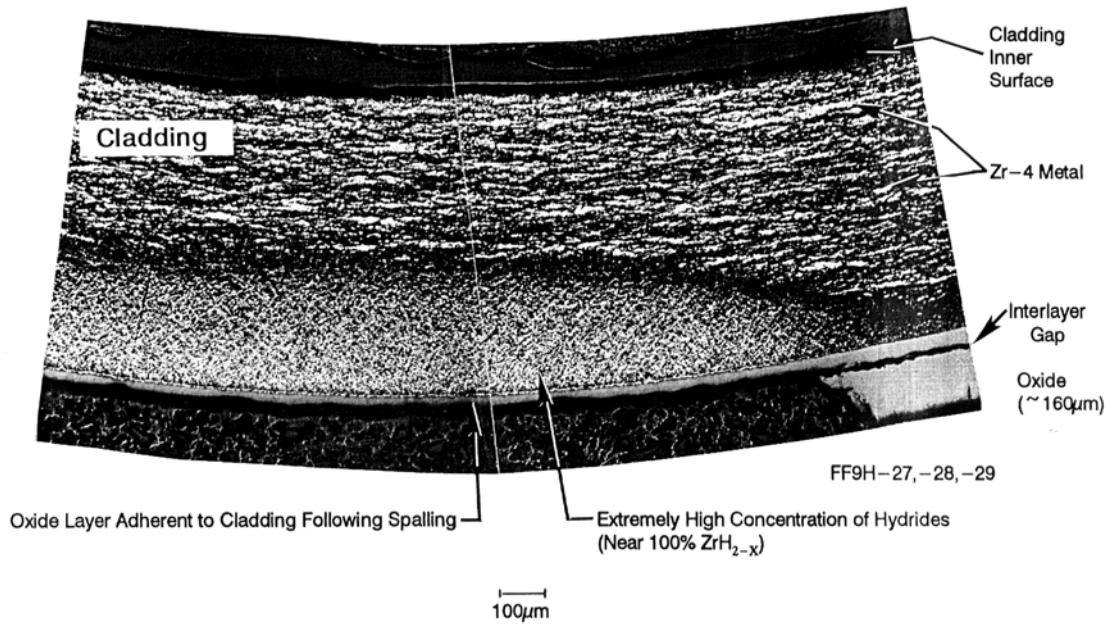

Figure 4-2 Solid hydride lens generated by oxide spallation

The effect of a stress gradient is very similar to that of a temperature gradient. The concentration of hydrogen in solution increases with increasing hydrostatic stress in the matrix. Thus, TSS is reached first at the highest stressed point in the matrix, commonly at the tip of a pre-existing crack in the material. Despite claims otherwise *Ref. 12* there is no stress effect on TSS (outside the range resulting from measurements errors in the partial molar volume measurements) *Ref. 13*. If both temperature and stress gradients are in conflict, the temperature gradient appears to be the stronger effect *Ref. 12.*

In theory, thermal cycling should have no effect in redistributing hydrides in zirconium alloys. However, because of the hysteresis between the hydride dissolution and precipitation curves; the relatively slow kinetics of both processes; and the different stress fields surrounding hydrides precipitated at different types of sites, during a heating phase hydrogen from a solid hydride layer on the material surface dissolves faster than hydrogen from small hydrides distributed along grain boundaries. This allows a concentration gradient to exist during the heating cycle. Reprecipitation occurs on the pre-existing grain boundary hydrides within the matrix. Thus, by repeated thermal cycling it is possible to dissolve surface hydride layers (or blisters) and produce a uniform hydride distribution that exceeds the expected average hydrogen concentration for TSS at the maximum temperature of the thermal cycles *Ref. 44.* This phenomenon was christened "supercharging" *Ref. 49-52* and can be a very useful technique for achieving high uniform hydrogen contents, or for redistributing hydride layers and blisters that may have formed in the material. The hydrogen fluxes necessary to override this "supercharging" effect have also been determined *Ref. 33.*

5 PARAMETERS IMPACTING BWR AND PWR HYDRIDING PICKUP BEHAVIOUR

In this section the different parameters impacting hydrogen pickup is discussed. Since the hydrogen pickup is a function of both corrosion rate and hydrogen pickup fraction, both these parameters are presented.

5.1 MICROSTRUCTURE

The importance of a high density of medium size second phase particles in the unirradiated material to get good corrosion and hydriding performance was reported by Rudling et al., 2000. In this study different Zr-2 BWR fuel claddings were irradiated in different Swedish BWRs, Table 5-1. Through somewhat different chemical compositions and different manufacturing routes, different second phase particle size distributions were obtained, Figure 5-1. The horizontal curves in the figure is an artefact due to that the resolution limit is about 50 nm. An increased SPP density of particles initially larger than 50 nm, decrease the hydriding rate, Figure 5-2. The reason for this decrease is the improved corrosion resistance with a larger density initially of particles larger then 50 nm, Figure 5-3. *Thus, the hydrogen pickup fraction is about the same for materials with large and small densities of particles larger than 50 nm.* The authors suggest that the existence of second phase particles larger than a critical size (25-50 nm in BWRs) is necessary to form a protective zirconium oxide barrier layer. More SPPs larger than this size will increase the barrier layer thickness. This barrier layer will ensure that both corrosion and hydriding rates are low. However, if the second phase particles becomes smaller than this critical size, both corrosion and hydriding rates will dramatically increase. Since there is a tendency for second phase particles dissolution in a BWR, the SPPs must be so large initially that at the end of life the second phase particles in the material is still larger than the critical size to formation this barrier layer.

Table 5-1: Summary of irradiation data, Rudling et al., 2000, Ref. 53.

Rod	Reactor	Fuel Type	Burnup, MWd/kgU	Fast Fluence, $E > 1$ MeV, $\times 10^{21}$ n/cm^2	EFPH	Average LHGR, kW/m	Average Surface Heat Flux, W/cm^2
a1	A	8 × 8	42	13.5	37 000	22	57.2
a2	A	8 × 8	44.5	14.1	42 000	22	57.2
a3	A	8 × 8	44	14.1	42 000	22	57.2
a4	A	10 × 10	38.5	12.1	33 000	17	56.3
b1	B	8 × 8	41.7	12.7	46 000	20	52
c1	C	8 × 8	44.5	15	45 000	20	52

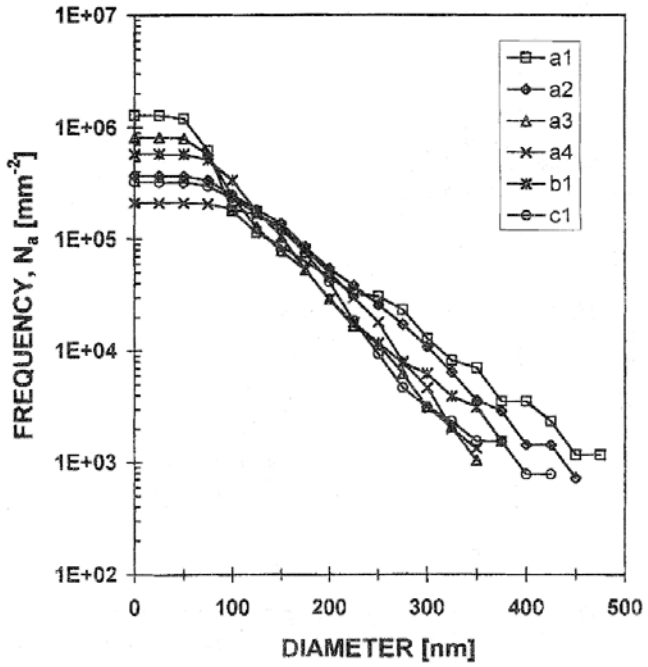

Figure 5-1: Comparison of cumulative SPP size distribution of the different unirradiated materials assessed in SEM. Each curve shows how many second phase particles per mm^2 that are larger than a certain size, Rudling et al., 2000, Ref. 53.

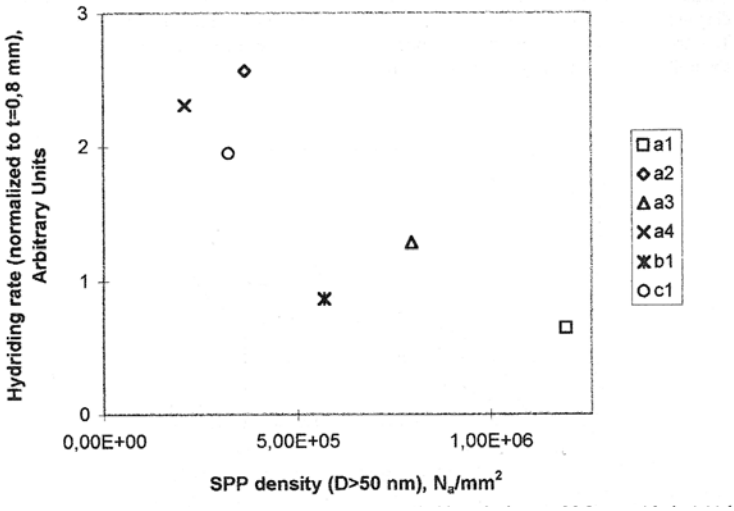

Figure 5-2: Variation of the hydriding rate normalised to a cladding thickness of 0.8 mm with the initial cumulative SPP density of particles larger than 50 nm, Rudling et al., 2000, Ref. 53.

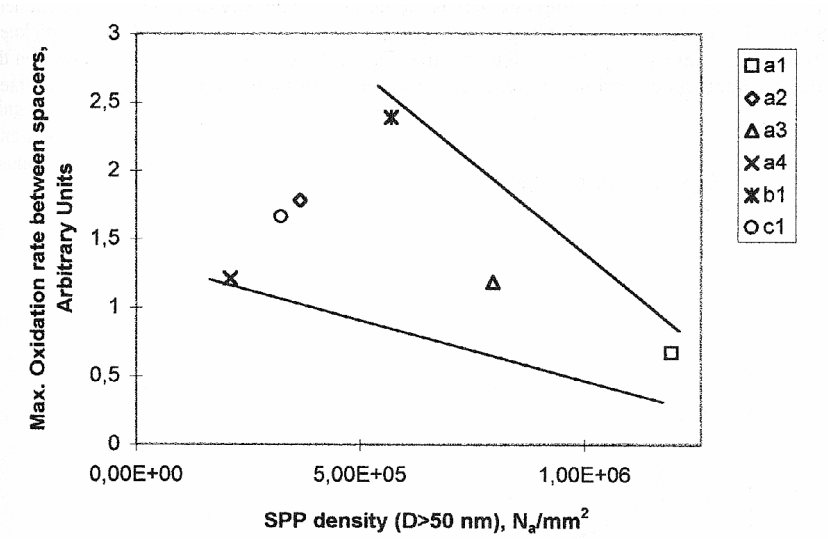

Figure 5-3: Variation of the maximum oxidation rate along the fuel cladding (except at spacer locations) in arbitrary units with the initial cumulative SPP density of particles larger than 50 nm, Rudling et al., 2000, Ref. 53.

Data presented by *Huang et al., 1996, Ref. 54*, indicated that if the precipitates in Zircaloy are almost lost the BWR corrosion and hydriding rates will increase dramatically. In the work of Huang et al, Zry-2 coupons were manufactured differently resulting in a large differences in second phase particle size distributions in the unirradiated materials, Figure 5-4.

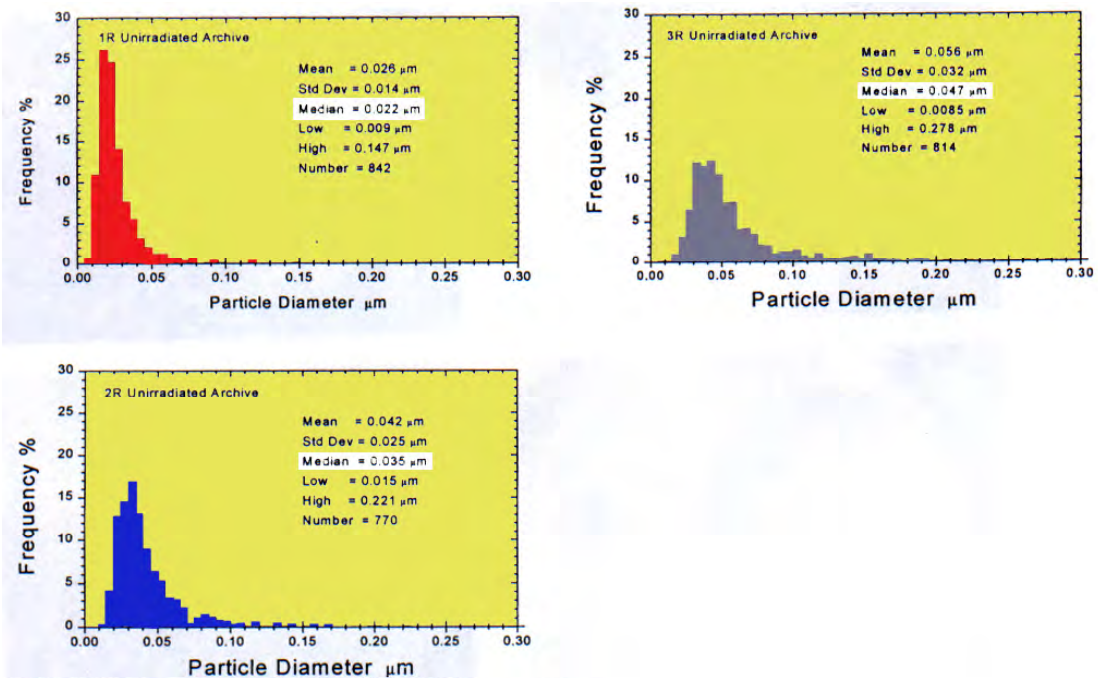

Figure 5-4: Precipitate size distribution of 1R, 2R and 3R GE Zry- 2 coupons, P. Y. Huang, et al. 1996, Ref. 54.

6 INFLUENCE OF HYDRIDES ON MATERIAL PERFORMANCE

In the following the impact of hydrides on fuel performance both during normal operation, class I and II transients and Design Basis Accidents such as LOCA and RIA are discussed.

6.1 NORMAL OPERATION AND CLASS I AND II TRANSIENTS

6.1.1 PCI/PCMI

During normal operation hydrides may decrease the ductility during a class I and II transients that the fuel clad may actually fail. During a transient the thermal heat expansion of the fuel pellet may result in tensile stresses in the cladding, Pellet Cladding Mechanical Interaction, PCMI. If this interaction occurs under the influence of iodine the mechanism is named, Pellet Cladding Interaction, PCI.

Garde et al., 1996, Ref. 64, investigated the impact of hydrides on ductility in Zry-4 claddings irradiated in two different PWR reactors. Different mechanical tests were performed at temperatures ranging from 313 to 673 K. The fast neutron dose in the materials were 9 to $12.3 \cdot 10^{21}$ n/cm^2 (E>1MeV)[4]. The tested materials had obtained an oxide thickness ranging from 12 to 114 μm, where specimens with an oxide thickness exceeding about 100 μm showed local oxide spalling. In these cases the local improved cooling (by the thinner oxide) resulted in a concentration of hydrides close to the cladding outer diameter, Figure 6-1. It is well-known that hydrogen diffuses from higher to lower temperatures, *Markowitz, 1961, Ref. 65, Kammenzind et al., 1996, Ref. 66.*

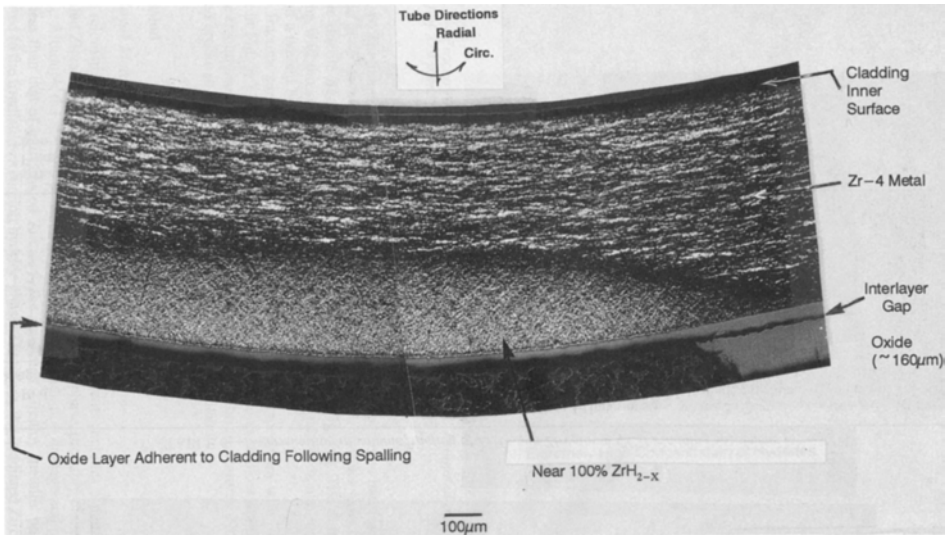

Figure 6-1: Concentration of zirconium hydrides at fuel clad outer diameter due to local oxide spalling, Garde et. al., 1996, Ref. 64.

[4] A fast neutron dose of $1 \cdot 10^{21}$ n/cm^2 (E>1MeV) corresponds to a burnup of about 10 MWd/kgU.

The results from the mechanical tests are shown in Figure 6-2 and Figure 6-3, where filled symbols represents the samples showing oxide spalling which in turn has resulted in concentration of hydrides at the clad outer diameter. It is indicated that samples with oxide spalling show less plasticity compared to specimens without oxide spalling. The four specimens showing oxide spalling did show a uniform deformation less than 0.5 %, Figure 6-2.

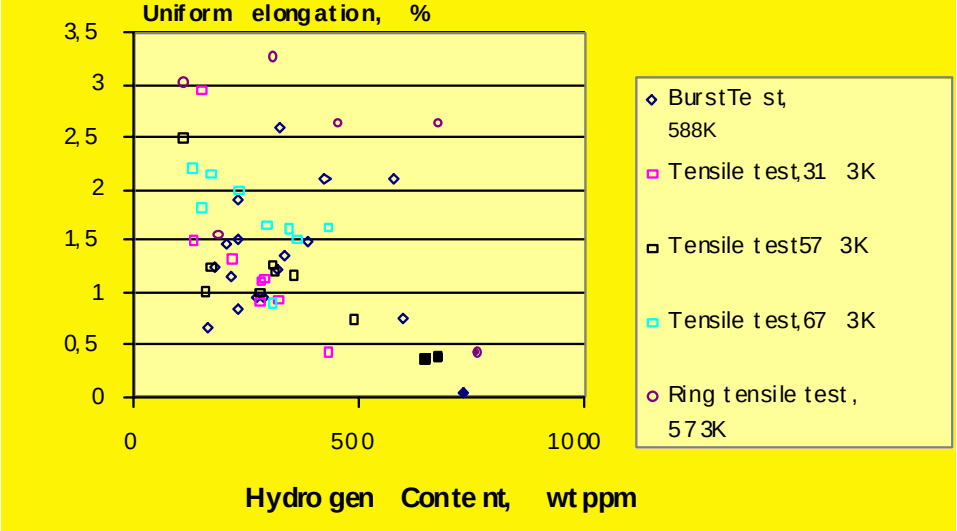

Figure 6-2: Impact of hydrogen content on uniform deformation in irradiated Zry-4. Filed symbols represents specimens with large local concentrations of hydrides at the clad outer diameter due to localised oxide spalling, Garde et al., 1996, Ref. 64.

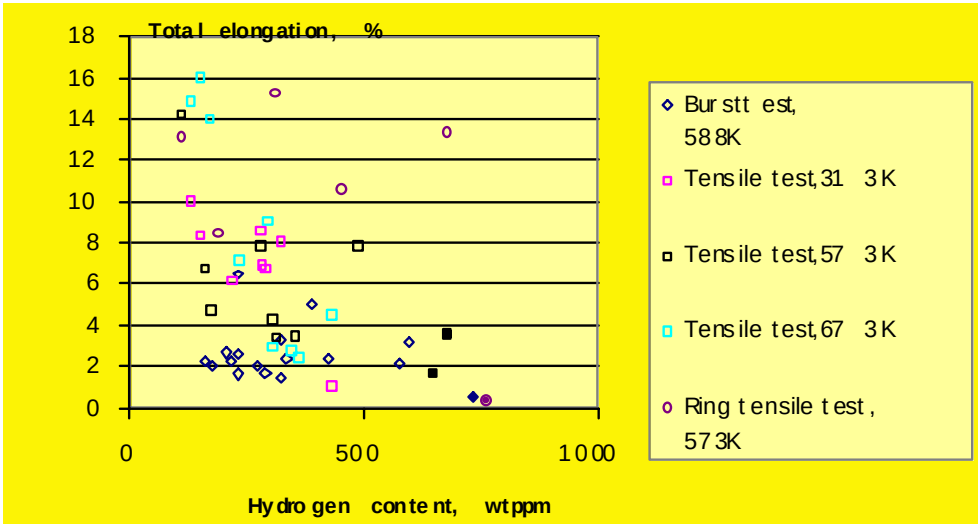

Figure 6-3: Impact of hydrogen content on total deformation in irradiated Zry-4. Filed symbols represents specimens with large local concentrations of hydrides at the clad outer diameter due to localised oxide spalling, Garde m. fl. , 1996, Ref. 64.

Rudling and Pettersson, 1998, Ref. 67, presented ramp data on heavily spalled PWR Zry-4 fuel cladding irradiated to a burnup of 35 MWd/kgU, Figure 6-4. The maximum hydrogen content in the fuel cladding was about 1100 wtppm (measured as an average value across the cladding thickness. Five fuel cladding segments were ramped to a maximum rod power of 45-50 kW/m without failing. However, subsequent hot-cell examinations showed cracks formed during the ramping at the clad outer diameter, Figure 6-5. The cracks had probably formed in this location since the outer diameter oxide thickness and the heavily hydrided area also at this location is much more brittle than the rest of the cladding. During the ramping process the resulting tensile stresses in the fuel cladding will consequently result in crack initiation and propagation at the clad outer diameter. The degree of crack propagation will partly depend on how much of the fuel cladding thickness is heavily hydrided. For a heavily hydrided fuel cladding through the major part of the fuel cladding thickness, the fuel cladding may fail during a power ramp. The authors suggest that the reason for that the fuel rods did not fail due to *PCI* or *PCMI* may be due to that the thick oxide (where the oxide had not spalled off) would result in a significantly high fuel cladding temperature making the fuel cladding material more ductile. This since the oxide thermal conductivity is so much lower than that of the zirconium alloy material.

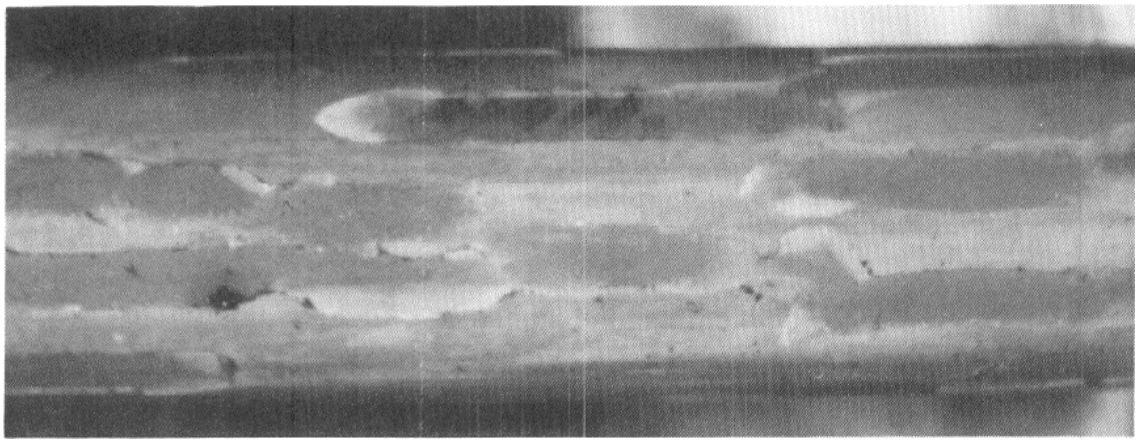

Figure 6-4: Example of fuel segmented rod showing excessive spalling, Rudling and Pettersson, 1998, Ref. 67.

7 REFERENCES

Ref. 1 *B. Lustman and F. Kerze, "The Metallurgy of Zirconium", Chapter 3, McGraw-Hill, N.Y., 1955.*

Ref. 2 *M.N.A. Hall, S.L.H. Martin and A.L.G. Rees, "The Solubility of Hydrogen in Zirconium and Zirconium-Oxygen Solid Solutions", Trans. Faraday Soc., 41 (1945) 306-325.*

Ref. 3 *E. Zuzek, J.P. Abrita, A. San-Martin and F.D. Manchester, "The Hydrogen-Zirconium System", Bull. of Alloy Phase Diagrams, 11 (1990) 385-395.*

Ref. 4 *W.M. Small, J.H. Root and D. Khatamian, "Observations of Kinetics of γ–Zirconium Hydride Formation in Zr-2.5%Nb by Neutron Diffraction", J. Nucl. Mater., 256 (1998) 102-107.*

Ref. 5 *J.J. Kearns, "Terminal Solubility and Partitioning of Hydrogen in the Alpha-Phase of Zirconium, Zircaloy-2 and Zircaloy-4", J. Nucl. Mater., 22 (1967) 304-310.*

Ref. 6 *Z.L. Pan, I.G. Ritchie and M.P. Puls, "The Terminal Solid Solubility of Hydrogen and Deuterium in Zr-2.5%Nb Alloys", J. Nucl. Mater., 228 (1996) 227-237.*

Ref. 7 *Z.L. Pan and M.P. Puls, "The effect of Cold Work on the Terminal Solubility of Hydrogen in Zirconium Alloys", Poster Presentation at 12th Int. Symp. on Zr in the Nucl. Ind., Abstract Book pp75/76.*

Ref. 8 *A. McMinn, E.C. Darby and J.S. Schofield, "The Terminal Solubility of Hydrogen in Zirconium Alloys", Proc. 12th Int. Symp. on Zr in the Nucl. Ind., Toronto, ON., 1998, ASTM-STP-1354, pp173-195.*

Ref. 9 *K.M. Tashiro, "Hydrogen Measurements by Differential Scanning Calorimetry", Ontario Hydro Research Review, No.8, 1993, pp29-30.*

Ref. 10 *S.L.H. Martin and A.L.G. Rees, "Interpretation of the Solubility of Hydrogen in Zirconium", Trans. Faraday Soc., 30 (1954) 343-352.*

Ref. 11 *B. Cox, "Hydrogen Trapping by Oxygen and Dislocations in Zirconium Alloys", J. Alloys and Comp., 256 (1997) L4-L7.*

Ref. 12 *B.F. Kammenzind, B.M. Berquist, R. Bajaj, P.H. Kreyns and D.G. Franklin, "The Long-Range Migration of Hydrogen Through Zircaloy in Response to Tensile and Compressive Stress Gradients", Proc. 12th Int. Symp. on Zr in the Nucl. Ind., Toronto, ON., 1998, ASTM-STP-1354, pp. 196-233.*

Ref. 13 *C.E. Coleman and J.F.R. Ambler, "Solubility of Hydrogen Isotopes in Stressed Hydride-Forming Metals", Scripta Met., 17 (1983) 77-82.*

Ref. 14 *A. Sawatzky, "Hydrogen in Zircaloy-2 : Its Distribution and Heat of Transport", J. Nucl. mater., 2 (1960) 321-328.*

Ref. 15 *A. Sawatzky and E. Vogt, "Mathematics of Thermal Diffusion of Hydrogen in Zircaloy-2", Trans. Met. Soc. AIME, 227 (1963) 917-928.*

Ref. 16 *G.V. Kidson, "A Review of Diffusion Processes in Zirconium and its Alloys", Electrochem. Tech., 4 (1966) 193-205.*

Ref. 17 *A. Sawatzky, G.A. Ledoux, R.L. Tough and C.D. Cann, "Hydrogen Diffusion in Zirconium-Niobium Alloys", Metal-Hydrogen Systems: Proc. of the Miami Int. Symp. 1981, Pergamon, Oxford (1982), pp109-120.*

Ref. 18 *R. Dutton, "A Layman's Guide to Radiation-Induced Deformation Processes in Zirconium Alloys", Atomic Energy of Canada Ltd., Report AECL - 10158 (July 1990).*

Ref. 19 *C.E. Ells, "Hydride Precipitates in Zirconium Alloys", J. Nucl. Mater., 28 (1968) 129-151.*

Ref. 20 *G.J.C. Carpenter, J.F. Watters and R.W. Gilbert, "Dislocations Generated by Zirconium Hydride in Zr and Some of its Alloys", J. Nucl. Mater.,48 (1973) 267-276.*

Ref. 21 *P. Bouffioux and N. Rupa, "Impact of Hydrogen on Plasticity and Creep of Unirradiated Zircaloy-4 Cladding Tubes", Proc. 12th Int. Symp. on Zr in the Nucl. Ind., Toronto, ON., 1998, ASTM-STP-1354, pp399-422.*

Ref. 22 *C. Roy, "Nucleation and Growth of Hydrides in Zirconium Alloys", Atomic Energy of Canada Ltd., Report AECL-2297 (Sept.1965).*

Ref. 23 *G.C. Weatherly, "The Precipitation of γ–Hydride Plates in Zirconium", Acta Met., 29 (1981) 501-512.*

Ref. 24 *W. Yeniscavich, R. A. Wolfe and R. M. Lieberman, Irradiation-Induced Hydrogen Absorption of Nickel-Enriched Zircaloy-2: The WAPD-29-14 Experiment, WAPD-T-912, 1958.*

Ref. 25 *C. L. Whitmarsh, Review of Zircaloy-2 and Zircaloy-4 Properties Relevant to N. S. Savannah Reactor Design, Oak Ridge Natinoal Laboratory Report No. ORNL-3281, UC-80-Reactor Technology, TID-4500 (17th ed.).*

Ref. 26 *S.-C. Lin and M. Hamasaki, The Effect of Dispersion and Spheroidisation Treatment of Zirconium Hydrides on the Mechanical Properties of Zircaloy, Nucl. Sc. and Eng., 71, 1979, 251-266.*

Ref. 27 *S. Arséne and J. Bai, Effect of Hydriding and Irradiation on the Mechanical Properties of Zircaloy Cladding, CNRS URA Report No. 850, 1998.*

Ref. 28 *D. O. Northwood and U. Kosasih, Hydrides and Delayed Hydrogen Cracking in Zirconium and its Alloys, Int. Met. Review, Vol 28, No. 2, 1983, 92-121.*

Ref. 29 *IAEA report, Review of Fuel Failures in Water Cooled Reactors, IAEA Report, Technical Report Series No. 388, IAEA, Vienna, 1998.*

Ref. 30 *K. Edsinger, A review of fuel degradation in BWRs, ANS Topical Meeting on LWR Fuel Performance, Park City, 2000.*

Ref. 31 *K. Edsinger, S. Vaidyanathan and R. B. Adamson, On the mechanism of axial splits in failed BWR fuel rods, Proc. 9th Environmental Degradation Conference, San Diego, 1999.*

Ref. 32 *E.A. Gulbansen and K.F. Andrew, "Kinetics of the Reactions of Zirconium with O_2, N_2 and H_2", Met. Trans., 185 (1949) 515-525.*

Ref. 33 *B. Cox, "Hydrogen Uptake During Oxidation of Zirconium Alloys", J. Alloys and Comp., 256 (1997) 244-246.*

Ref. 34 *B. Cox, "A Mechanism for the Hydrogen Uptake Process in Zirconium Alloys", J. Nucl. Mater., 264 (1999) 283-294.*

Ref. 35 *B. Cox and Y-M. Wong, "A Hydrogen Uptake Micro-Mechanism for Zr Alloys", J. Nucl. Mater., 270 (1999) 134-146.*

Ref. 36 *B. Cox, "Corrosion and Hydriding of Zircaloy Fuel Cladding", Proc. 6th Int. Conf. on CANDU Fuel, Niagara Falls, ON., Sept.1999, Vol. 2, pp338-347, Can. Nuclear Soc.*

Ref. 37 *P. Bossis, G. Lelièvre, P. Barbaris, X, Iltis and F. Lefèbvre, "Multi-Scale Characterisation of the Metal-Oxide Interface of Zirconium Alloys", Proc. 12th Int. Symp. on Zr in the Nucl. Ind., Toronto, ON., 1998, ASTM-STP-1354, pp918-945.*

Ref. 38 *P. Rudling and G. Wikmark, "A unified model of Zircaloy BWR corrosion and hydriding mechanisms", J. Nucl. Mater., 265 (1999) 44-59.*

Ref. 39 *IAEA-TECDOC-996, 1998*

Ref. 40 *P. Bossis, G. Lelièvre, P. Barberis, X. Iltis and F. Lefebvre, Multi-Scale Characterisation of the Metal Oxide Interface of Zirconium Alloys, Zirconium in the Nuclear Industry: Twelfth International Symposium, ASTM STP 1354, G. Sabol and G. Moan, Eds. American Society for Testing and Materials, West Conshohocken, PA, 2000, pp. 918-945.*